

# Statistical Taylor Expansion: A New and Path-Independent Method for Uncertainty Analysis \*

Chengpu Wang

40 Grossman Street, Melville, NY 11747, USA

Chengpu@gmail.com

January 27, 2026

## Abstract

As a rigorous statistical approach, statistical Taylor expansion extends the conventional Taylor expansion by replacing precise input variables with random variables of known distributions and sample counts to compute the mean, the standard deviation, and the reliable factor of each result. It tracks the propagation of the input uncertainties through intermediate steps, so that the final analytic result becomes path independent. Therefore, it differs fundamentally from common approaches in applied mathematics that optimize computational path for each calculation. Statistical Taylor expansion may standardize numerical computations for analytic expressions. This study also introduces the implementation of statistical Taylor expansion termed variance arithmetic and presents corresponding test results across a wide range of mathematical applications.

Another important conclusion of this study is that numerical errors in library functions can significantly affect results. It is desirable that each value from library functions be accomplished by an uncertainty deviation.

**Keywords:** computer arithmetic, error analysis, interval arithmetic, uncertainty, numerical algorithms.

**AMS subject classifications:** G.1.0

Copyright ©2024

## 1 Introduction

Let  $x$  and  $\delta x$  be a value and its uncertainty deviation, respectively. As an input,  $x$  and  $\delta x$  are the mean and standard deviation of a measurement [1][2]. If  $\delta x = 0$ ,  $x$  is a *precise value*, otherwise, the pair specifies an *imprecise value*  $x \pm \delta x$ .

Let  $P(x) \equiv \delta x/|x|$  be the *statistical precision* (hereafter referred to as precision) of  $x \pm \delta x$ . A smaller  $P(x)$  indicate a higher measurement quality of  $x \pm \delta x$ , and when

---

\*

$P(x) \ll 1$ , it is unclear whether  $\delta x$  is too poor to measure  $x$ , or it is a measurement of  $x = 0$ .

Statistical Taylor expansion determines the result  $f \pm \delta f$  of a general analytic expression  $f(x, \dots)$ , and the reliability  $\alpha \in [0, 1]$  of  $f \pm \delta f$  based on the inputs  $x \pm \delta x, \dots$  and their corresponding sample counts.

- Previous studies have examined the effect of input uncertainties on output values for specific cases [3]. Statistical Taylor expansion generalizes these effects as uncertainty bias, as shown in Formula (2.5) and (2.8) in this paper.
- The traditional variance-covariance framework accounts only for linear interactions between random variables through an analytic function [3][4][5], whereas statistical Taylor expansion extends this framework to include higher-order interactions as expressed in Formula (2.9) in this paper.
- Calculating the reliability of  $f \pm \delta f$  seems completely new.

Statistical Taylor expansion is superior to all existing numerical arithmetic.

Conventional floating-point arithmetic [6][7][8] can only calculate the result  $f$  which contains unknown amount of rounding error [9][10][11]. As a consequence, a floating-point representation with  $10^{-16}$  resolution may not be good enough for inputs with  $10^{-2}$  to  $10^{-6}$  precision. While statistical Taylor expansion can track rounding errors.

The bounding range in interval arithmetic [12][13][14][15][16] is inconsistent with the statistical nature of an  $x \pm \delta x$  pair and it tends to over-estimate the result uncertainty due to its worst-case assumption [17]. On the other hand, statistical Taylor expansion is precise statistically.

Both conventional floating-point arithmetic and interval arithmetic depend strongly on the specific algebraic form of an analytic function, a phenomenon known as the *dependency problem* [10][11][12][14], which makes the numerical calculations of analytic problems sometimes more like an art than science. In contrast, statistical Taylor expansion is path independent.

To be rigorous in mathematics and statistics, statistical Taylor expansion abandons the significance arithmetic nature of its processor [17].

As a statistical sampling process, stochastic arithmetic [18][19] is computationally expensive, while statistical Taylor expansion provides a direct characterization without sampling.

In this paper:

1. Section 1 compares briefly statistical Taylor expansion with all other numerical arithmetic.
2. Section 2 develops the theoretical foundation of statistical Taylor expansion.
3. Section 3 describes variance arithmetic as a numerical implementation of statistical Taylor expansion.
4. Section 4 lays out standard to validate variance arithmetic.
5. Section 5 illustrates variance arithmetic in computing polynomial, demonstrating its capability in tracing floating-point rounding errors, and its continuity in parameter space.
6. Section 6 applies variance arithmetic to adjugate matrix and matrix inversion, showing that the uncertainty calculation for a linear calculation is no longer linear. It also distinguishes between a distribution test and a value test.

7. Section 7 evaluates variance arithmetic on common mathematical library functions. It also shows that the error deviation should be close to 1 except near a distributional pole.
8. Section 8 reveals the accumulation of numerical errors by reusing an input multiple time in a moving-window progressive algorithm.
9. Section 9 showcases variance arithmetic in catching catastrophic cancellation in a regression algorithm.
10. Section 10 examines the impact of numerical library errors and shows that these errors can be significant.
11. Section 11 concludes with a summary and a discussion.

## 2 Statistical Taylor Expansion

### 2.1 The Uncorrelated Uncertainty Condition

When there is no systematic error [1][2] among the inputs, the uncertainties of the inputs are uncorrelated to each other, even though the inputs may have significant correlations among them. This condition can be characterized quantitatively in statistics as the *uncorrelated uncertainty condition* [17].

### 2.2 Distributional Zero and Distributional Pole

Let  $\rho(\tilde{x}, \mu, \sigma)$  denote the probability density function of a random variable  $\tilde{x}$  with the distribution mean  $\mu$  and distribution deviation  $\sigma$ . Let  $\tilde{y} = f(\tilde{x})$  be a strictly monotonic function, so that its inverse function  $\tilde{x} = f^{-1}(\tilde{y})$  exists. Formula (2.1) shows the probability density function of  $\tilde{y}$  [1][4]. In Formula (2.1), the same distribution can be expressed in terms of either  $\tilde{x}$  or  $\tilde{y}$ , which are simply different representations of the same underlying random variable.

$$\rho(\tilde{x}, \mu, \sigma)d\tilde{x} = \rho(f^{-1}(\tilde{y}), \mu, \sigma) \frac{d\tilde{x}}{d\tilde{y}}d\tilde{y} = \rho(\tilde{y}, \mu_y, \sigma_y)d\tilde{y}; \quad (2.1)$$

Viewed in the  $f^{-1}(\tilde{y})$  coordinate,  $\rho(\tilde{y}, \mu_y, \sigma_y)$  is given by  $\rho(\tilde{x}, \mu, \sigma)$  modulated by  $1/f_x^{(1)}$ , in which  $f_x^{(1)}$  is the first derivative of  $f(x)$  with respect to  $x$ .

- A *distributional pole* occurs when  $f_x^{(1)} = 0 \rightarrow \rho(\tilde{y}, \mu_y, \sigma_y) = \infty$ . For example,  $(\mu \pm 1)^2$  has a distributional pole at  $\tilde{x} = 0$ , as shown in Figure 1.
- A *distributional zero* occurs when  $f_x^{(1)} = \infty \rightarrow \rho(\tilde{y}, \mu_y, \sigma_y) = 0$ . For example  $\sqrt{\mu \pm 1}$  has a distributional zero at  $\tilde{x} = 0$ , as shown in Figure 2.

In both Figure 1 and 2,  $\rho(\tilde{y}, \mu_y, \sigma_y)$  closely representation resembles  $\rho(\tilde{x}, \mu, \sigma)$  when the mode of  $\rho(\tilde{x}, \mu, \sigma)$  lies sufficiently far away from either a distributional pole or a distributional zero, such as  $(5 \pm 1)^2$  in Figure 1 and  $\sqrt{5 \pm 1}$  in Figure 2, thereby allowing for characterization of the output  $f(x)$  using mean  $\overline{f(x)}$  and deviation  $\delta f(x)$  only.

### 2.3 Statistical Taylor Expansion

Define  $\tilde{z} \equiv (\tilde{x} - \mu)/\sigma$  and let  $\rho(\tilde{z})$  be the normalized form of  $\rho(\tilde{x}, \mu, \sigma)$  such that  $\tilde{z}$  has distribution mean 0 and distribution deviation 1.

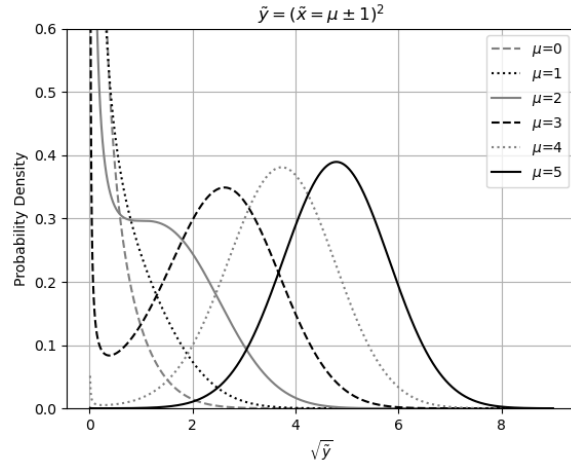


Figure 1: Probability density function of  $\tilde{y} = \tilde{x}^2$ , for various values of  $\mu$  as indicated in the legend. The variable  $\tilde{x}$  follows a Gaussian distribution with mean  $\mu$  and deviation 1. The horizontal axis is scaled as  $\sqrt{\tilde{y}}$ .

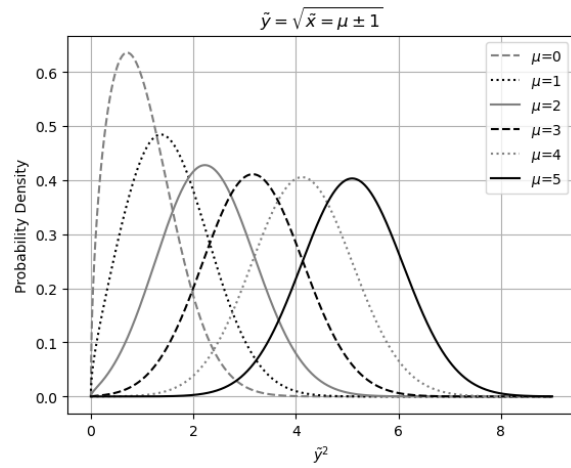


Figure 2: Probability density function for  $\tilde{y} = \sqrt{\tilde{x}}$ , various values of  $\mu$  as indicated in the legend. The variable  $\tilde{x}$  follows a Gaussian distribution with the distributional mean  $\mu$  and deviation 1. The horizontal axis is scaled as  $\tilde{y}^2$ .

$$\zeta(n) \equiv \int_{\varrho}^{\kappa} \tilde{z}^n \rho(\tilde{z}) d\tilde{z}; \quad (2.2)$$

$$\zeta(1) = 0; \quad (2.3)$$

Let  $\tilde{z} \in [\varrho, \kappa]$  where  $\varrho, \kappa$  specify the *bounding ranges*. Formula (2.2) defines the corresponding *bound moment*  $\zeta(n)$ , which further satisfies the *mean-reverting condition* of Formula (2.3) so that  $\kappa$  determines  $\varrho$ . For any symmetric  $\rho(-\tilde{z}) = \rho(\tilde{z}) : \varrho = -\kappa, \zeta(2n+1) = 0$ . The probability of  $\tilde{z} \notin [\varrho, \kappa]$  is defined as the *bounding leakage*  $\epsilon(\kappa) = 1 - \zeta(0, \kappa)$ .

$$f(x + \tilde{x}) = f(x + \tilde{z}\sigma) = f(x) + \sum_{n=1}^{\infty} \frac{f_x^{(n)}}{n!} \tilde{z}^n \sigma^n; \quad (2.4)$$

$$\overline{f(x)} = \int_{-\varrho}^{+\kappa} f(x + \tilde{x}) \rho(\tilde{x}, \mu, \sigma) d\tilde{x} = f(x) + \sum_{n=1}^{\infty} \sigma^n \frac{f_x^{(n)}}{n!} \zeta(n); \quad (2.5)$$

$$\begin{aligned} \delta^2 f(x) &= \overline{(f(x) - \overline{f(x)})^2} = \overline{f(x)^2} - \overline{f(x)}^2 \\ &= \sum_{n=1}^{\infty} \sigma^n \sum_{j=1}^{n-1} \frac{f_x^{(j)}}{j!} \frac{f_x^{(n-j)}}{(n-j)!} (\zeta(n) - \zeta(j)\zeta(n-j)); \end{aligned} \quad (2.6)$$

An analytic function  $f(x)$  can be accurately evaluated over in a range using the Taylor series as shown in Formula (2.4). Formula (2.5) and Formula (2.6) yield the mean  $\overline{f(x)}$  and the variance  $\delta^2 f(x)$  of  $f(x)$ , respectively. The difference  $\overline{f(x)} - f(x)$  is defined as the *uncertainty bias*, representing the effect of input uncertainty on the resulting value.

$$f(x + \tilde{x}, y + \tilde{y}) = \sum_{m=0}^{\infty} \sum_{n=0}^{\infty} \frac{f_{(x,y)}^{(m,n)}}{m!n!} \tilde{x}^m \tilde{y}^n; \quad (2.7)$$

$$\overline{f(x, y)} = \sum_{m=0}^{\infty} \sum_{n=0}^{\infty} (\sigma_x)^m (\sigma_y)^n \frac{f_{(x,y)}^{(m,n)}}{m!n!} \zeta_x(m) \zeta_y(n); \quad (2.8)$$

$$\begin{aligned} \delta^2 f(x, y) &= \sum_{m=1}^{\infty} \sum_{n=1}^{\infty} (\sigma_x)^m (\sigma_y)^n \sum_{i=0}^m \sum_{j=0}^n \frac{f_{(x,y)}^{(i,j)}}{i!j!} \frac{f_{(x,y)}^{(m-i,n-j)}}{(m-i)!(n-j)!} \\ &\quad (\zeta_x(m)\zeta_y(n) - \zeta_x(i)\zeta_x(m-i)\zeta_y(j)\zeta_y(n-j)); \end{aligned} \quad (2.9)$$

Under the uncorrelated uncertainty condition, Formula (2.8) and (2.9) compute the mean and variance of the Taylor expansion given in Formula (2.7), where  $\zeta_x(m)$  and  $\zeta_y(n)$  denote the variance moments for  $x$  and  $y$ , respectively. Although Formula (2.9) is only for 2-dimensional, it can be extended easily to any dimension.

With the mean reverting condition of Formula (2.3):

$$\overline{x \pm y} = \zeta(0, \kappa_x) x \pm \zeta(0, \kappa_x) y; \quad (2.10)$$

$$\delta^2(x \pm y) = \zeta(2, \kappa_x) (\sigma_x)^2 + \zeta(2, \kappa_y) (\sigma_y)^2; \quad (2.11)$$

$$\overline{xy} = \zeta(0, \kappa_x) x \zeta(0, \kappa_y) y; \quad (2.12)$$

$$\delta^2(xy) = \zeta(2, \kappa_x) (\sigma_x)^2 y^2 + x^2 \zeta(2, \kappa_y) (\sigma_y)^2 + \zeta(2, \kappa_x) (\sigma_x)^2 \zeta(2, \kappa_y) (\sigma_y)^2; \quad (2.13)$$

When  $N \rightarrow \infty$ ,  $\zeta(0, \kappa) \rightarrow 1$  and  $\zeta(2, \kappa) \rightarrow 1$ , making Formula (2.10) and (2.11) the convolution results for  $x \pm y$  [4], and Formula (2.12) and (2.13) the corresponding results of the product distribution for  $xy$  [4].

## 2.4 One-Dimensional Examples

Formula (2.14) and (2.15) give the mean and variance for  $e^x$ , respectively:

$$\frac{\overline{e^x}}{e^x} = 1 + \sum_{n=1}^{\infty} \sigma^n \zeta(n) \frac{1}{n!}; \quad (2.14)$$

$$\frac{\delta^2 e^x}{(e^x)^2} = \sum_{n=2}^{\infty} \sigma^n \sum_{j=1}^{n-1} \frac{\zeta(n) - \zeta(j)\zeta(n-j)}{j!(n-j)!}; \quad (2.15)$$

Formula (2.16) and (2.17) give the mean and variance for  $\log(x)$ , respectively:

$$\overline{\log(x)} = \log(x) + \sum_{n=1}^{+\infty} P(x)^n \frac{(-1)^{n+1} \zeta(n)}{n}; \quad (2.16)$$

$$\delta^2 \log(x) = \sum_{n=2}^{+\infty} P(x)^n \sum_{j=1}^{n-1} \frac{\zeta(n) - \zeta(j)\zeta(n-j)}{j(n-j)}; \quad (2.17)$$

Formula (2.19) and (2.20) give the mean and variance for  $\sin(x)$ , respectively:

$$\sin(x + \tilde{x}) = \sum_{n=0}^{\infty} \eta(n, x) \frac{\tilde{x}^n}{n!}; \quad \eta(n, x) \equiv \begin{cases} n = 4j : & \sin(x); \\ n = 4j + 1 : & \cos(x); \\ n = 4j + 2 : & -\sin(x); \\ n = 4j + 3 : & -\cos(x); \end{cases} \quad (2.18)$$

$$\overline{\sin(x)} = \sum_{n=0}^{\infty} \sigma^n \eta(n, x) \frac{\zeta(n)}{n!}; \quad (2.19)$$

$$\delta^2 \sin(x) = \sum_{n=2}^{\infty} \sigma^n \sum_{j=1}^{n-1} \frac{\eta(j, x)\eta(n-j, x)}{j!(n-j)!} (\zeta(n) - \zeta(j)\zeta(n-j)); \quad (2.20)$$

Formula (2.21) and (2.22) give the mean and variance for  $x^c$ , respectively:

$$\frac{\overline{x^c}}{x^c} = 1 + \sum_{n=1}^{\infty} P(x)^n \zeta(n) \binom{c}{n}; \quad (2.21)$$

$$\frac{\delta^2 x^c}{(x^c)^2} = \sum_{n=2}^{\infty} P(x)^n \sum_{j=1}^{n-1} \binom{c}{j} \binom{c}{n-j} (\zeta(n) - \zeta(j)\zeta(n-j)); \quad (2.22)$$

The input and output in statistical Taylor expansion reflects the inherent characteristics of the calculation, such as  $\sigma \rightarrow P(e^x)$ ,  $P(x) \rightarrow \delta \log(x)$ ,  $\sigma \rightarrow \delta \sin(x)$ , and  $P(x) \rightarrow P(x^c)$ .

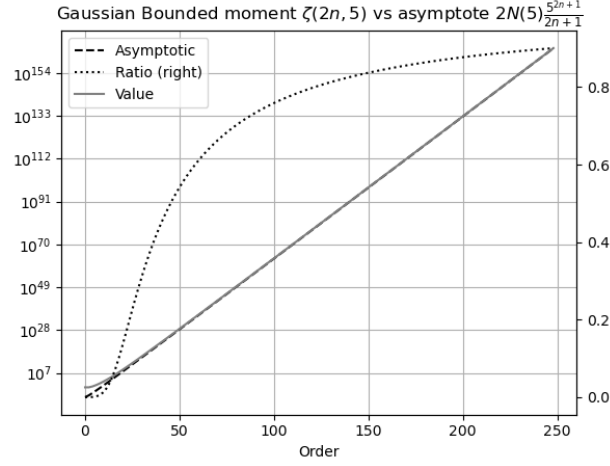


Figure 3: When  $\kappa = 5$ , the value of bound moment  $\zeta(2n, \kappa)$  (left y-axis) for Gaussian distribution with order  $2n$  (x-axis) versus  $2N(\kappa) \frac{\kappa^{2n+1}}{2n+1}$  (left y-axis), and their ratio (right y-axis).

## 2.5 Convergence of Variance

$$\zeta(2n, \kappa) = \int_{-\kappa}^{+\kappa} \bar{z}^{2n} \frac{1}{2\sqrt{3}} d\bar{z} = 2\rho(\kappa) \frac{\kappa^{2n+1}}{2n+1}, \quad 0 \leq \kappa \leq \sqrt{3}; \quad (2.23)$$

$$\lim_{n \rightarrow +\infty} \zeta(2n, \kappa) = 2\rho(\kappa) \frac{\kappa^{2n+1}}{2n+1}; \quad (2.24)$$

$$\forall j : \lim_{n \rightarrow +\infty} \zeta(n) - \zeta(j)\zeta(n-j) = \frac{\kappa^n}{n}; \quad (2.25)$$

$$\rho(-\bar{z}) = \rho(\bar{z}) : \delta^2 \log(x \pm \delta x) \sim \sum_{n=1}^{+\infty} \frac{(P(x)\kappa)^{2n}}{(2n)^2}; \quad (2.26)$$

$$\rho(-\bar{z}) = \rho(\bar{z}) : \frac{\delta^2 (x \pm \delta x)^c}{(x^c)^2} \sim \sum_{n=1}^{+\infty} (P(x)\kappa)^{2n} \frac{\binom{2c}{2n}}{2n}; \quad (2.27)$$

Formula (2.25) shows that the asymptotic behavior of  $\zeta(n, \kappa)$  when  $n \rightarrow \infty$  determines if Formula (2.6) will converge. For example, Formula (2.23) gives  $\zeta(2n, \kappa)$  for Uniform distributions, Formula (2.24) shows the asymptoticity for any symmetric distribution  $\rho(\bar{z})$ , and Figure 3 shows  $\zeta(2n, 5)$  for Normal distribution when  $2n \rightarrow +\infty$ .

- Formula (2.15) for  $e^{x \pm \delta x}$  and Formula (2.20) for  $\sin(x \pm \delta x)$  both converge unconditionally.
- Formula (2.17) for  $\log(x \pm \delta x)$  can be approximated by Formula (2.26), which converges when  $P(x) < 1/\kappa$ . Statistical Taylor expansion rejects the distributional zero of  $\log(x)$  or  $(x \pm \delta x)^c$  in the range of  $P(x) \gtrsim 1/\hat{\kappa}$  statistically due

to the divergence of Formula (2.26) and (2.27) mathematically, with  $\zeta(2n, \hat{\kappa})$  providing the connection between these two perspectives.

- Formula (2.22) for  $(x \pm \delta x)^c$  can be approximated by Formula (2.27). which converges when  $P(x) \lesssim 1/\kappa$  although the precise upper bound for  $P(x)$  varies with  $c$ .

## 2.6 Statistical Bounding

When sampling from a distribution, the sample mean  $\bar{x}$  and sample deviation  $\delta x$  approach the distribution mean  $\mu$  and distribution deviation  $\sigma$  respectively as the sample count  $N$  increases [4]. This yields the *sample bounding leakage*  $\epsilon(\kappa, N)$  for the interval  $[\bar{x} - \varrho\delta x, \bar{x} + \kappa\delta x]$ , in contrast to the *distributional bounding leakage*  $\epsilon(\kappa)$  for the interval  $[\mu - \varrho\sigma, \mu + \kappa\sigma]$ . Because  $\epsilon(\kappa) \neq \epsilon(\kappa, N)$  for finite  $N$ , let  $\epsilon(\kappa) = \epsilon(\kappa_s, N)$ , where  $\kappa_s$  is the *measuring bonding range*, and  $\kappa(\kappa_s, N)$  is the *measured bounding range*.

$$\epsilon(\kappa) = 1 - \xi\left(\frac{\kappa}{\sqrt{2}}\right); \quad (2.28)$$

$$\epsilon(\kappa_s, N) = 1 - \frac{1}{2}\xi\left(\frac{|\kappa_s\delta x - \bar{x}|}{\sqrt{2}}\right) - \frac{1}{2}\xi\left(\frac{|\kappa_s\delta x + \bar{x}|}{\sqrt{2}}\right); \quad (2.29)$$

When the underlying distribution is Normal, Formula (2.28) and (2.29) give the distributional bounding leakage  $\epsilon(\kappa)$  and the sample bounding leakage  $\epsilon(\kappa_s, N)$  respectively, where  $\xi(\cdot)$  is the Normal error function [4]. Figure 4 shows that  $\epsilon(\kappa_s) < \epsilon(\kappa_s, N)$ , and  $\lim_{N \rightarrow \infty} \epsilon(\kappa_s, N) = \epsilon(\kappa_s)$  along the y-axis direction. It also shows that  $\kappa(\kappa_s, N) < \kappa_s$  and  $\lim_{N \rightarrow \infty} \kappa(\kappa_s, N) = \kappa_s$  along the x-axis direction. Figure 5 further demonstrates that for smaller  $\kappa_s$ ,  $\kappa(\kappa_s, N)$  approaches  $\kappa_s$  more rapidly as  $N$  increases, but converges to a larger stable bounding leakage  $\epsilon(\kappa_s)$ .

When the underlying distribution is uniform, the portion of sampled range  $[\bar{x} - \sqrt{3}\delta x, \bar{x} + \sqrt{3}\delta x]$  outside the actual range  $[\mu - \sqrt{3}\sigma, \mu + \sqrt{3}\sigma]$  contributes to the bounding leakage  $\epsilon(N)$ . Figure 5 shows that  $0 < \epsilon(N) \sim N^{-0.564}$  empirically. The measured bounding range  $\kappa(N) = \sqrt{3}(1 - \epsilon(N))$ .

## 2.7 Ideal Statistics

$$\zeta(2, \kappa) = \frac{\delta^2 x}{(\delta x)^2}; \quad (2.30)$$

$$\alpha(x \pm y) = \frac{\zeta_x(2, \kappa_x)(\delta x)^2 + \zeta_y(2, \kappa_y)(\delta y)^2}{(\delta x)^2 + (\delta y)^2}; \quad (2.31)$$

When sample count  $N \rightarrow \infty$ ,  $\zeta(0) \rightarrow 1$ ,  $\zeta(2) \rightarrow 1$  and  $\delta^2 x \rightarrow (\delta x)^2$  in Formula (2.30). Such relationship of  $\delta^2 f$  versus sample count  $N$  is general:

- When the underlying uncertainty distribution is Gaussian and  $\kappa_s = 5$ , Figure 6 shows that the resulting variances  $\delta^2 f$  for a selected functions rise with  $N$  until reaching the corresponding stable values  $\widehat{\delta^2 f}$  when  $N \geq 50$ .
- When the underlying uncertainty distribution is Uniform,  $\kappa_s = \sqrt{3}$ , Figure 7 shows the same trend, however the stable variances  $\widehat{\delta^2 f}$  are reached only when  $N \geq 10^4$ .

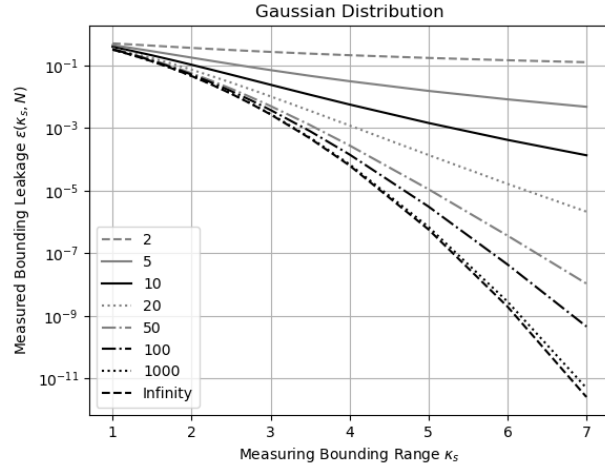


Figure 4: Measured bounding leakage  $\epsilon(\kappa_s, N)$  (y-axis) for varying measuring bounding range  $\kappa_s$  (x-axis) and sample count  $N$  (legend).

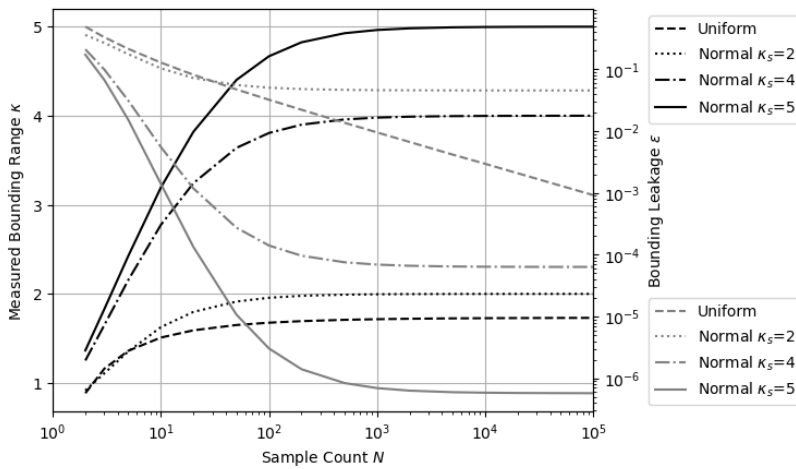


Figure 5: Measured bounding range  $\kappa$  (left y-axis) and corresponding measured bounding leakage  $\epsilon(\kappa)$  (right y-axis) for varying sample count  $N$  (x-axis) when the underlying distribution is uniform or normal (legend), with different measuring bounding range  $\kappa_s$  for the normal distribution.

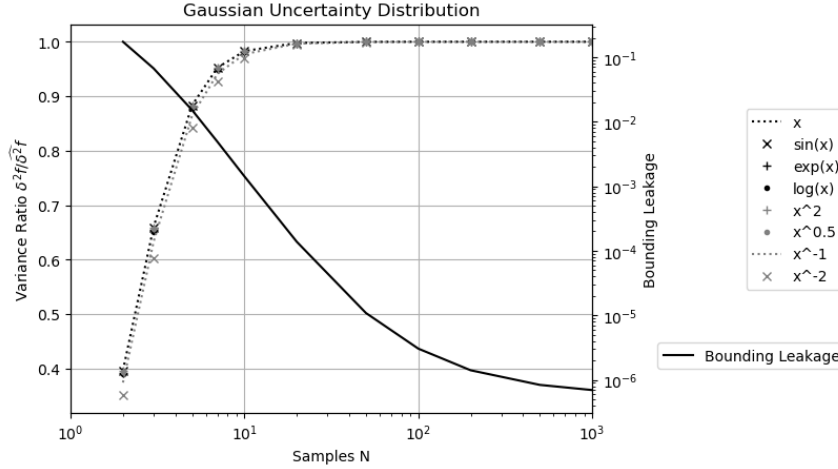


Figure 6: The ratio of resulting variance  $\delta^2 f$  to the ideal variance  $\widehat{\delta^2 f}$  (left y-axis) and the bounding leakage (right y-axis) for varying sample count  $N$  (x-axis) for the selected function  $f(x = 1 \pm 0.1)$  (legend) when the uncertainty distribution is Gaussian.

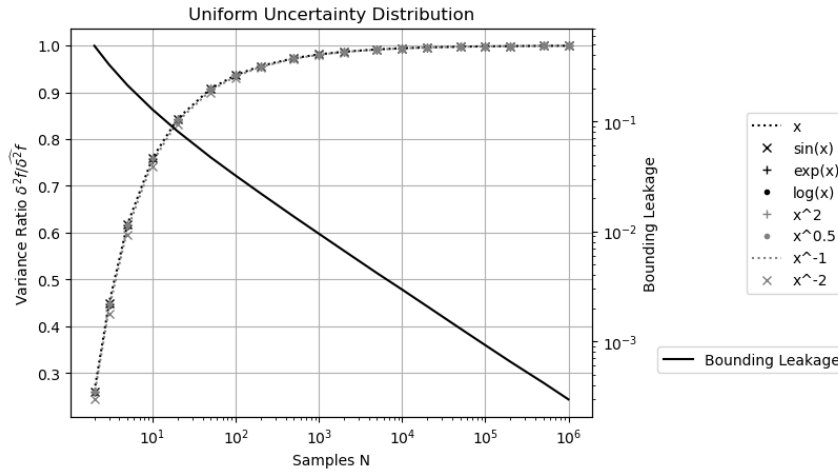


Figure 7: The ratio of resulting variance  $\delta^2 f$  to the ideal variance  $\widehat{\delta^2 f}$  (left y-axis) and the bounding leakage (right y-axis) for varying sample count  $N$  (x-axis) for the selected function  $f(x = 1 \pm 0.1)$  (legend) when the uncertainty distribution is Uniform.

The trends of uncertainty biases  $\bar{f} - f$  versus sample count  $N$  are exactly as those in Figure 6 and 7 respectively, except that  $\bar{x} - x = 0$ . This similarity is expected because the first-order approximation in both Formula (2.5) and Formula (2.6) contains  $\sigma^2\zeta(2, \kappa)$ .

In both Figure 6 and 7, the bonding leakage  $\epsilon(N)$  decreases as the sample count  $N$  increases. The stable resulting variances  $\widehat{\delta^2}f$  is reached only when  $\epsilon(s, N) < 10^{-3}$ . All functions approach their corresponding stable variances with exactly the same trend in each figure. These observations suggest that bounding leakage is the reason for  $\delta^2 f < \widehat{\delta^2} f$  and it is justified to infer the confidential interval range  $\kappa$  from bounding leakage  $\epsilon(\kappa_s) = 1 - \zeta(0, \kappa_s)$  in Figure 4, or more precisely  $1 - \zeta(2, \kappa_s)$  for  $\delta^2 f$ .

Define the stable variance when the sample count  $N$  is sufficiently large as the *ideal variance*  $\widehat{\delta^2}f$ . The choice of  $\kappa_s$  to calculate  $\widehat{\delta^2}f$  is defined as the ideal bounding range  $\hat{\kappa}$ . For Uniform distribution, by definition  $\hat{\kappa} = \sqrt{3}$ . When the input distribution is unbounded, the choice of  $\hat{\kappa}$  is a trade-off: a larger  $\hat{\kappa}$  means a smaller bounding leakage for the result but a narrower convergence range for the input. For Gaussian distribution, according to the 5- $\sigma$  rule for determining the statistical significance of experimental result [1][2][4],  $\hat{\kappa} = 5$ .

When the sample count  $N$  is insufficient,  $\widehat{\delta^2}f$  is calculated using  $\hat{\kappa}$ , to assume that  $N$  is sufficient.  $\delta^2 f$  is calculated with the actual  $N$ . Define the *ideal ratio* as  $\alpha \equiv \delta^2 f / \widehat{\delta^2} f$ , which is 0 when  $N = 1$  and 1 when  $N$  is sufficiently large. The ideal ratio  $\alpha$  quantifies the reliability of  $\widehat{\delta^2}f$  from the underlying distributions and the corresponding sample counts of all inputs, with Formula (2.31) as an example for  $\alpha(x \pm y)$ .

## 2.8 Dependency Tracing

$$\delta^2(f + g) = \delta^2 f + \delta^2 g + 2(\overline{fg} - \bar{f}\bar{g}); \quad (2.32)$$

$$\delta^2(c_1 f + c_0) = c_1^2 \delta^2 f; \quad (2.33)$$

When all inputs satisfy the uncorrelated uncertainty assumption, statistical Taylor expansion traces dependencies through the intermediate steps. For example:

- Formula (2.32) expresses  $\delta^2(f + g)$ . The dependency tracing of is illustrated by  $\delta^2(f - f) = 0$ , and  $\delta^2(f(x) + g(y)) = \delta^2 f + \delta^2 g$ , with the latter corresponding to Formula (2.11).
- The dependence tracing of  $\delta^2(fg)$  is illustrated by  $\delta^2(f/f) = 0$ ,  $\delta^2(ff) = \delta^2 f^2$ , and  $\delta^2(f(x)g(y)) = \bar{f}^2(\delta^2 g) + (\delta^2 f)\bar{g}^2 + (\delta^2 f)(\delta^2 g)$ , with the latter corresponding to Formula (2.13).
- The dependency tracing of  $\delta^2 f(g(x))$  is demonstrated by  $\delta^2(f^{-1}(f(x))) = (\delta x)^2$ . For a reversible transformation such as matrix reversion or FFT, after a *round-trip transformation* which is a forward transformation followed by a reverse transformation, the original input should be restored.
- Formula (2.33) gives the variance of the linear transformation of a function, which can be applied to other formulas for more general dependency tracing.

Statistical Taylor expansion employs dependency tracing to ensure that the calculated mean and variance satisfy statistics rigorously. Dependency tracing also implies that the results of statistical Taylor expansion must remain path independent. However, dependency tracing comes at a cost: variance calculations are generally more complex than value calculations and exhibits a narrower convergence range for input variables.

## 2.9 Traditional Execution and Dependency Problem

Dependency tracing requires an analytic form of the function to apply statistical Taylor expansion for the result mean and variance, as in Formula (2.5), (2.6), (2.8), and (2.9). This requirement often conflicts with conventional numerical methods for analytic functions:

- Traditionally, intermediate variables are widely used in computations; however, this practice disrupts dependency tracing by obscuring the relationships among the original input variables.
- Similarly, conditional executions are often employed to optimize performance and minimize rounding errors, for example, using Gaussian elimination to minimize floating-point rounding errors in matrix inversion [20]. For dependency tracing, such conditional executions should instead be replaced by direct matrix inversion as described in Section 6.
- Furthermore, traditional approaches frequently apply approximations to result values during execution. Under the statistical Taylor expansion, Formula (2.6) shows that the variance converges more slowly than value in statistical Taylor expansion. Consequently, approximation strategies should prioritize variances than values.
- Traditionally, results from mathematical library functions are accepted without scrutiny, with accuracy assumed down to the last digit. As demonstrated in Section 10, statistical Taylor expansion enables the detection of numerical errors within these functions and requires that they be recalculated with uncertainty deviations explicitly incorporated into the output.
- In conventional practice, an analytic expression is often decomposed into simpler, ostensibly and independent arithmetic operations such as negation, addition, multiplication, division, square root, and library calls. However, this decomposition introduces dependency problems. For example, if  $x^2 - x$  is calculated as  $x^2 - x$ ,  $x(x - 1)$ , and  $(x - \frac{1}{2})^2 - \frac{1}{4}$ , only  $(x - \frac{1}{2})^2 - \frac{1}{4}$  gives the correct result, while the other two give wrong results for wrong independence assumptions between  $x^2$  and  $x$ , or between  $x - 1$  and  $x$ , respectively.
- Similarly, large calculations are often divided into sequential steps, such as computing  $f(g(x))$  as  $f(y)|_{y=g(x)}$ . This approach also introduces the dependency problem by ignoring dependency tracing within  $g(x)$  affecting  $f(g(x))$ , such as  $\overline{(\sqrt{x})^2} > \overline{\sqrt{x^2}}$  and  $\delta^2(\sqrt{x})^2 > \delta^2\sqrt{x^2}$ .

Dependency tracing therefore removes nearly all flexibility from traditional numerical executions, effectively eliminating the associated dependency problems. Consequently, all conventional numerical algorithms must be reevaluated or redesigned to align with the principles of statistical Taylor expansion.

## 3 Variance Arithmetic

Variance arithmetic implements statistical Taylor expansion. It represents an imprecise value  $x \pm \delta x$  using a pair of 64-bit standard floating-point numbers and uses floating-point arithmetic for computation.

Because of the finite precision and limited range of conventional floating-point representation,  $\zeta(n)$  can only be computed to limited terms. Consequently, the following numerical rules are introduced:

- *finite*: The resulting value and variance must remain finite.
- *monotonic*: As a necessary condition for convergence, the last 20 terms of the expansion must decrease monotonically in absolute value, ensuring that the probability of the expansion exhibiting an absolute increase is no more than  $2^{-20} \simeq 9.53 \cdot 10^{-7}$ .
- *stable*: To avoid truncation error [5], the absolute value of the last expansion term must be less than  $\epsilon$  times of both the result deviation and the result absolute value, in which  $\epsilon \simeq 5.73 \cdot 10^{-7}$  is the bounding leakage for Gaussian distribution with  $\hat{\kappa} = 5$ . This rule ensures sufficiently fast convergence in the context of monotonic convergence.
- *positive*: At every expansion order, the expansion variance must be positive.
- *reliable*: At every order, the deviation of the variance must be less than 1/5 times the value of the variance.

For simplicity of discussion, the Taylor coefficients in Formula (2.4) and (2.7) are assumed to be precise.

### 3.1 Monotonic

Beyond an upper bound  $\delta x$ , the expansion is no longer monotonic for  $e^{x \pm \delta x}$ ,  $\log(x \pm \delta x)$ , and  $(x \pm \delta x)^c$ .

For Gaussian input uncertainty with  $\hat{\kappa} = 5$ :

- For  $e^{x \pm \delta x}$ ,  $\delta x \lesssim 19.864$  and  $P(e^{x \pm \delta x}) \lesssim 1681.767$  regardless of  $x$ . These limits follow directly from the relationship  $\delta x \rightarrow P(e^x)$ , as indicated in Formula (2.15).
- For  $\log(x \pm \delta x)$ ,  $P(x) \lesssim 0.20086$  and  $\delta \log(x \pm \delta x) \lesssim 0.213$  regardless of  $x$ . These limits follow directly from the relationship  $P(x) \rightarrow \delta \log(x)$ , as indicated in Formula (2.17).
- For  $(x \pm \delta x)^c$ , except when  $c$  is a natural number, the upper bound  $P(x)$  is close to 1/5 but increasing with  $c$ . This trend is displayed in Figure 8.

Similar trends holds when the input uncertainty is uniform but with different values. For example, after the respective upper bound  $P(x)$  for  $(x \pm \delta x)^c$  are normalized by the corresponding  $\hat{\kappa}$ , they show almost the same trends of increasing with  $c$ . Figure 9 shows the upper bound  $P(x)$  for  $(x \pm \delta x)^c$ .

### 3.2 Positive

Besides convergence, the variance expansion may yield negative results, as in Formula (2.20) for  $\sin(x \pm \delta x)$ . Figure 10 shows that the upper bound of  $\delta x$  for  $\sin(x \pm \delta x)$  varies periodically between  $0.318\pi$  and  $0.416\pi$  for Gaussian input uncertainty. Beyond this upper bound, the result deviation is no longer positive at some expansion order. Conceptually, the upper-bound for  $\delta x$  should not be much more than  $\pi/2$  to make the result meaningful, which Figure 10 satisfies. Similar trend holds when the input uncertainty is uniform but with larger upper bound  $\delta x$ , as shown in Figure 11.

### 3.3 Floating-Point Rounding Errors

Variance arithmetic incorporates floating-point rounding errors as the  $\delta x$  when converting a floating-point value  $x$  into  $x \pm \delta x$ . Unless all the least 20 bits of the significand

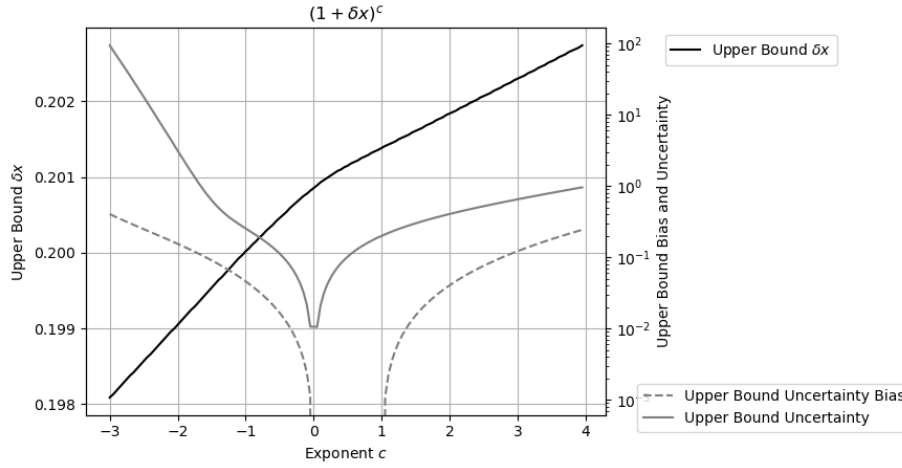


Figure 8: Measured upper bound  $\delta x$  (left y-axis) for  $(1 \pm \delta x)^c$  across different values of  $c$  (x-axis) for Gaussian uncertainty. The corresponding uncertainty bias and uncertainty are also shown (right y-axis). The x-axis is expressed in units of  $\pi$ . When  $c$  is a natural number,  $\delta x$  has no upper bound; however, such cases are omitted in the figure.

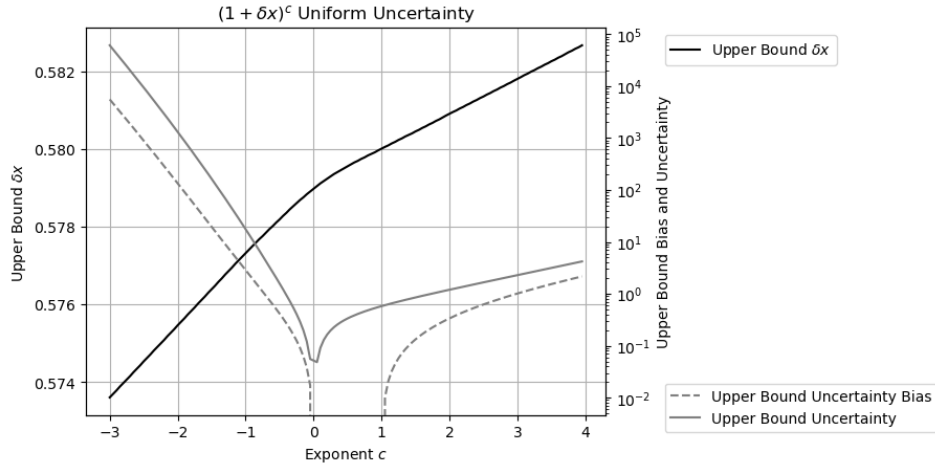


Figure 9: Measured upper bound  $\delta x$  (left y-axis) for  $(1 \pm \delta x)^c$  across different values of  $c$  (x-axis) for uniform uncertainty. The corresponding uncertainty bias and uncertainty are also shown (right y-axis). The x-axis is expressed in units of  $\pi$ . When  $c$  is a natural number,  $\delta x$  has no upper bound; however, such cases are omitted in the figure. When  $c \in [0, 1]$ , uncertainty bias is negative so it does not show up in the plot.

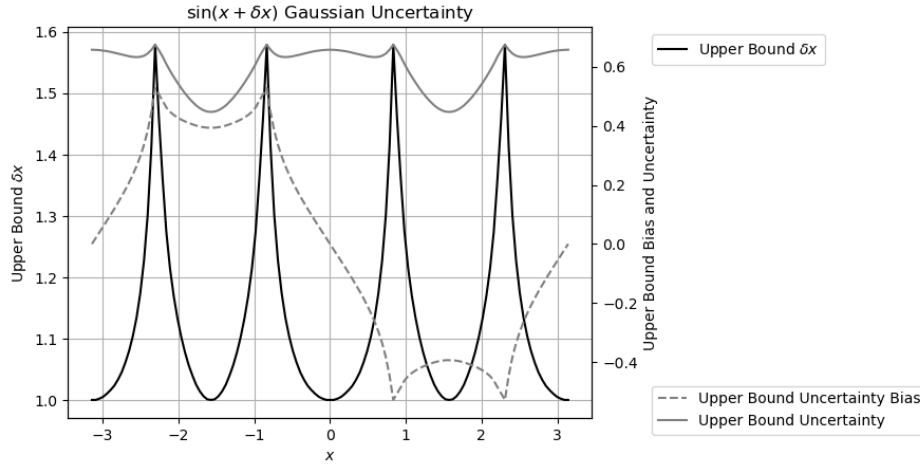


Figure 10: Measured upper bound  $\delta x$  (left y-axis) for  $\sin(x \pm \delta x)$  across different values of  $x$  (x-axis) for Gaussian uncertainty. The corresponding uncertainty bias and uncertainty are also shown (right y-axis). The x-axis is expressed in units of  $\pi$ .

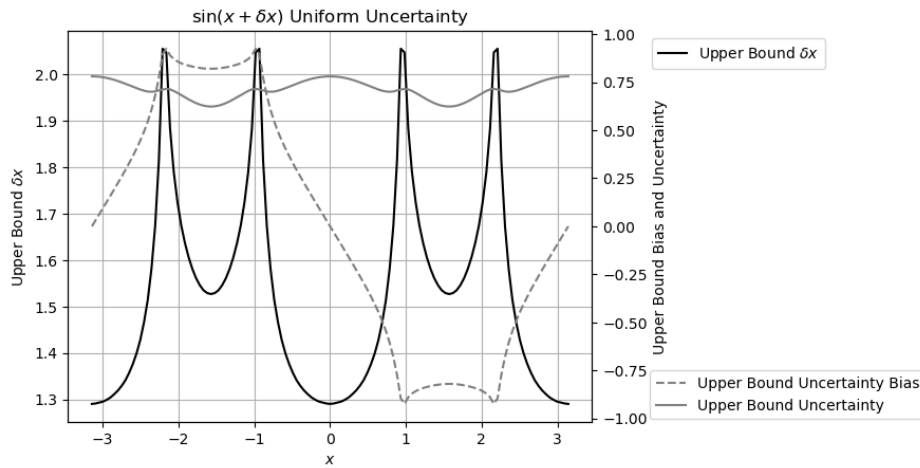


Figure 11: Measured upper bound  $\delta x$  (left y-axis) for  $\sin(x \pm \delta x)$  across different values of  $x$  (x-axis) for uniform uncertainty. The corresponding uncertainty bias and uncertainty are also shown (right y-axis). The x-axis is expressed in units of  $\pi$ .

of  $x$  are zero,  $\delta x$  is assumed to be  $1/\sqrt{3}$  times of the ULP of  $x$ , where ULP refers to the *Unit in the Last Place* in conventional floating-point representation [8], because rounding errors are shown to be uniformly distributed within ULP [17].

### 3.4 Comparison

Two imprecise values can be compared statistically based on their difference.

When the value difference is zero, the two imprecise values are considered equal. In statistics, such two values have a 50% possibility of being either less than or greater to each other but zero probability of being exactly equal [4]. In variance arithmetic, however, they are treated as neither less nor greater than each other and therefore are considered equal.

Otherwise, the standard z-statistic method [4] is applied to determine whether two imprecise values are statistically equal, less than, or greater than each other. For example, the difference between  $1.002 \pm 0.001$  and  $1.000 \pm 0.002$  is  $0.002 \pm 0.00224$ , yielding  $z = 0.002/0.00224$ . The probability that they are not equal is  $\xi(|z|/\sqrt{2}) = 62.8\%$ , in which  $\xi(z)$  is the cumulative distribution function for Normal distribution [4]. If the threshold probability for inequality is set at 50%, then  $1.000 \pm 0.002 < 1.002 \pm 0.001$ . Alternatively, an equivalent bounding range for  $z$  can be used, such as  $|z| \leq 0.67448975$  for an equal probability threshold of 50%.

Because the result of comparison depends on threshold probability which is application specific, comparison is not part of variance arithmetic.

## 4 Verification of Variance Arithmetic

Analytic functions or algorithms with precisely known results are used to evaluate the outputs of variance arithmetic based on the following statistical properties:

- *Value error*: the difference between the numerical result and the corresponding known precise analytic result.
- *Normalized error*: the ratio of a value error to the corresponding result deviation from statistical Taylor expansion.
- *Error deviation*: the standard deviation of normalized errors.
- *Error distribution*: the histogram of the normalized errors.

Once input error from every source is accounted precisely, *ideal coverage* is achieved in either contexts:

- *Distribution Test*: When comparing the calculated mean and deviation with the result data set, the error deviation is exactly 1 and the error distribution is Normal. Empirically, error distributions are close to Normal when error deviation are close to 1, regardless of input uncertainty distribution, and such convergence occurs rapidly [17]. This is due to central limit theorem [4].
- *Value Test*: When comparing the calculated value and the result value in a corresponding data set, the error deviation is much less than 1 and the error distribution is Delta. For example, a round-trip test is a value test.

However, if the input uncertainty is known only to order of magnitude, *proper coverage* is achieved when the error deviations fall within the range [0.1, 10].

When an input contains unspecified errors, such as numerical errors in library functions or floating-point rounding errors, Gaussian noise with progressively increasing

deviations can be added, until ideal coverage is attained. The minimal noise deviation required provides a good estimate of the magnitude of the unspecified input uncertainty deviations. Achieving ideal coverage serves as a necessary verification step to ensure that statistical Taylor expansion has been applied correctly within the given context. The input noise range that yields ideal coverage defines the ideal application range for the analytic function.

## 5 Polynomial

Formula (5.1) presents polynomial Taylor expansion:

$$\sum_{j=0}^N c_j (x + \tilde{x})^j = \sum_{j=0}^N \tilde{x}^j P_j, \quad P_j \equiv \sum_{k=0}^{N-j} x^{k-j} c_{j+k} \binom{j+k}{j}; \quad (5.1)$$

Because the maximal expansion term using Formula (5.1) is  $\tilde{x}^{2N}$ ,  $N$  in Formula (5.1) can only reach half of the maximal expansion order of Formula (2.6), for example,  $224 = 448/2$  when the input uncertainty is assumed to be Gaussian.

### 5.1 Residual Error

Figure 12 shows the residual error of  $\sum_{j=0}^{224} x^j - 1/(1-x)$ . It also displays the required expansion orders for  $1/(1-x)$ , which are all less than 224. Therefore, the residual error reflects solely the rounding error between  $\sum_{j=0}^{224} x^j$  and  $\frac{1}{1-x}$ . A detailed analysis indicates that the maximal residual error is 4 times the ULP of  $1/(1-x)$ . In all cases, the calculated uncertainty bounds the residual error effectively for all  $x$ , with an error deviation of 2.60 when the expansion order is less than 224. Variance arithmetic can provide proper coverage for rounding errors.

### 5.2 Continuity

In variance arithmetic, the result mean, variance and histogram are generally continuous across parameter space. For example,  $\delta x$  has an upper bound for  $(x \pm \delta x)^c$  to converge except when  $c$  is a natural number  $n$ . The result mean, variance and histogram of  $(x \pm \delta x)^c$  remain continuous around  $c = n$ .

### 5.3 Distributional Hole

Unlike a distributional zero, a statistical bounding range in variance arithmetic can include a distributional pole, such as around  $(0 \pm \delta x)^c, c > 1$ . The presence of such poles does not disrupt the continuity of the result mean, variance, or histogram. Figure 13 illustrates the error distributions of  $(x \pm 0.2)^n$  when  $x = 0, -0.2, +0.2$  and  $n = 2, 3$ .

- When the second derivative is zero, the resulting distribution is symmetric two-sided and Delta-like, such as when  $n = 3, x = 0$ .
- When the second derivative is positive, the resulting distribution is right-sided Delta-like, such as the distribution when  $n = 2, x = 0$ , or when  $n = 2, x = \pm 0.2$ , or when  $n = 3, x = 0.2$ .
- When the second derivative is negative, the resulted distribution is left-sided and Delta-like, such as when  $n = 3, x = -0.2$ , which is the mirror image of the distribution when  $n = 3, x = 0.2$ .

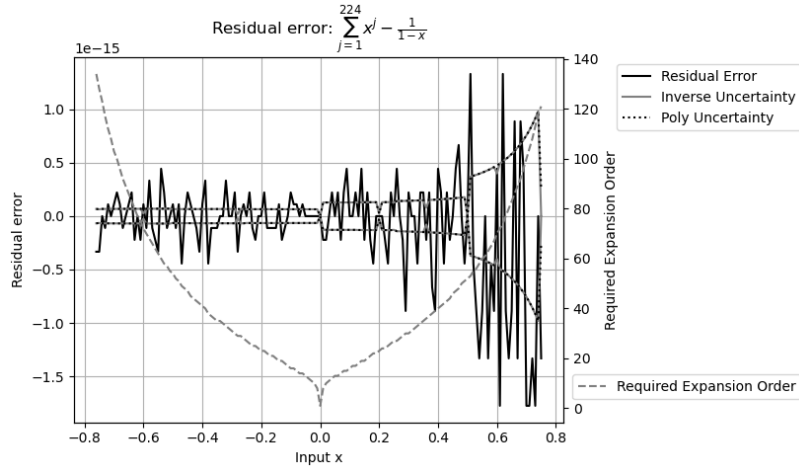


Figure 12: Residual error of  $\sum_{j=0}^{224} x^j - \frac{1}{1-x}$  vs  $x$  (x-axis). The y-axis to the left shows both the value and the uncertainty of the residual errors. The y-axis to the right indicates the expansion order needed to reach stable value for each  $x$ .

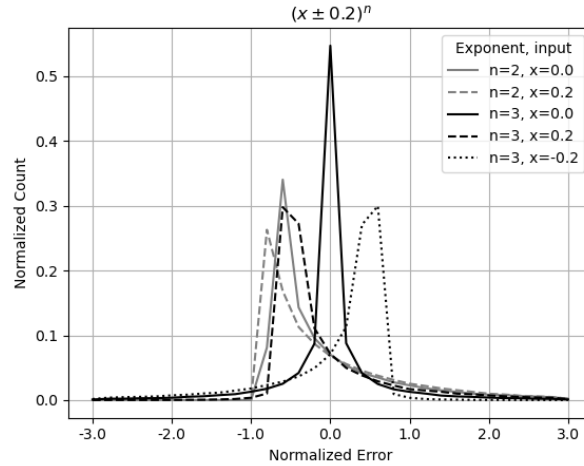


Figure 13: Histograms of normalized errors for  $(x \pm 0.2)^n$ , with  $x = 0, -0.2, +0.2$ , and  $n = 2, 3$ , as indicated in the legend.

In each case, the transition from  $x = 0$  to  $x = 0.2$  is continuous for the resulting mean and deviation.

## 6 Matrix Calculations

$$\overline{|\mathbf{M}|} = |\mathbf{M}|; \quad (6.1)$$

$$\delta^2 |\mathbf{M}| = \sum_{m=1}^n \sum_{\langle i_1 \dots i_m \rangle_n} \sum_{[j_1 \dots j_m]_n} |\mathbf{M}_{\langle i_1 \dots i_m \rangle_n, [j_1 \dots j_m]_n}|^2 \prod_{k=1 \dots n}^{i_k \in \{i_1 \dots i_m\}} (\delta x_{i_k, j_k})^2; \quad (6.2)$$

Let  $[j_1, j_2 \dots j_m]_n$  denote a permutation of length  $m$  from the vector  $(1, 2 \dots n)$ , and let  $\langle j_1, j_2 \dots j_m \rangle_n$  for the ordered permutation of length  $m$  [20]. Formula (6.1) and (6.2) gives the statistical Taylor expansion of the determinant of a square matrix  $\mathbf{M}$  of size  $n$ , when the uncertainties of matrix elements are all independent of each other. In Formula (6.2),  $\mathbf{M}_{\langle i_1 \dots i_m \rangle_n, [j_1 \dots j_m]_n}$  is a sub-matrix for  $\mathbf{M}$ , in which  $\langle i_1 \dots i_m \rangle_n$  contains the row indices, and  $[j_1 \dots j_m]_n$  contains the column indices.

The square matrix whose element is  $(-1)^{i+j} |m_{j,i}|$  is defined as the *adjugate matrix* [20]  $\mathbf{M}^A$  to the original square matrix  $\mathbf{M}$ , in which  $m_{j,i}$  is the element of  $\mathbf{M}$  at row index  $j$  and column index  $i$ . Each  $m_{j,i}$  is an integer between  $[-2^8, +2^8]$  so that  $\mathbf{M}^A$  can be calculated precisely using integer arithmetic. By adding Gaussian noise of deviation  $\delta x$  to each  $m_{j,i}$ ,  $\widetilde{\mathbf{M}}$  is created. The value error of  $\mathbf{M}^A$  is the difference between  $\widetilde{\mathbf{M}}^A$  and  $\mathbf{M}^A$ , while the result deviation is calculated by Formula (6.2), so that  $\widetilde{\mathbf{M}}^A - \mathbf{M}^A$  is a distribution test. Figure 14 shows that the error deviations of  $\widetilde{\mathbf{M}}^A - \mathbf{M}^A$  are very close to 1 except when the matrix size is 8 and the input uncertainty is  $\delta x = 10^{-17}$ . This abnormality is caused by floating-point rounding errors only at this point, when the element values exceed the significant range of 64-bit floating-point representation, to result in a error deviation of 3.2. Figure 14 demonstrates a typical distribution test of error deviation versus input noise deviation  $\delta x$  and another specific dimension, with ideal coverage for all region except when  $\delta x \rightarrow 0$ .

$$\mathbf{M} \times \mathbf{M}^A = \mathbf{M}^A \times \mathbf{M} = |\mathbf{M}| \mathbf{I}; \quad (6.3)$$

$$\mathbf{M}^{-1} \equiv \mathbf{M}^A / |\mathbf{M}|; \quad (6.4)$$

$$\delta^2 \begin{pmatrix} w, x \\ y, z \end{pmatrix}^{-1} \simeq \frac{\begin{pmatrix} z^4, x^2 z^2 \\ y^2 z^2, x^2 y^2 \end{pmatrix} (\delta w)^2 + \begin{pmatrix} y^2 z^2, w^2 z^2 \\ y^4, w^2 y^2 \end{pmatrix} (\delta x)^2}{(wz - xy)^4} + \frac{\begin{pmatrix} x^2 z^2, x^4 \\ w^2 z^2, w^2 x^2 \end{pmatrix} (\delta y)^2 + \begin{pmatrix} x^2 y^2, w^2 x^2 \\ w^2 y^2, w^4 \end{pmatrix} (\delta z)^2}{(wz - xy)^4}; \quad (6.5)$$

Let  $\mathbf{I}$  be the identity matrix for  $\mathbf{M}$  [20]. Formula (6.3) show the relation of  $\mathbf{M}^A$  and  $\mathbf{M}$  which leads to the definition of inverse matrix  $\mathbf{M}^{-1}$  in Formula (6.4) [20].  $\widetilde{\mathbf{M}} \times \widetilde{\mathbf{M}}^A - |\widetilde{\mathbf{M}}| \mathbf{I}$  tests each element value so that it is a value test. Figure 15 shows the error deviation of a typical value test: the error deviation decreases linearly with increasing input uncertainty deviation  $\delta x$ , because the value should match unless at  $\delta x \rightarrow 0$  when floating-point rounding errors dominate. The matrix size is the specific dimension in Figure 15.

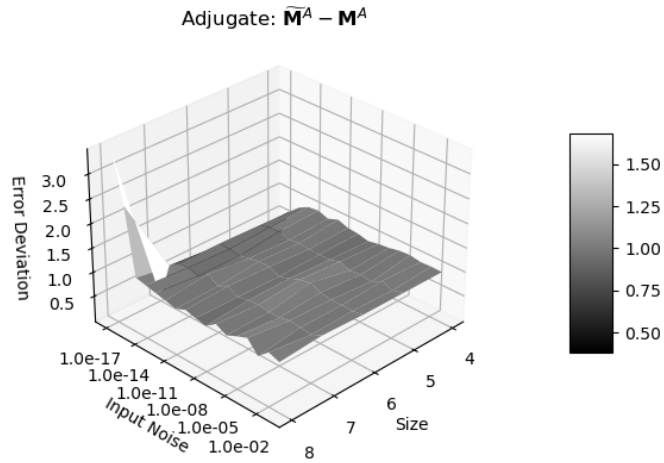


Figure 14: Error deviations (z-axis) of adjugate matrix  $\widetilde{\mathbf{M}}^A - \mathbf{M}^A$  as a function of matrix size (x-axis) and input noise precision (y-axis).

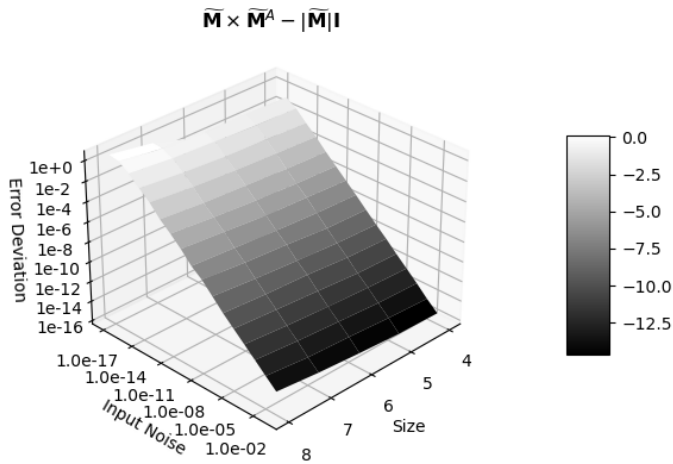


Figure 15: Error deviations (z-axis) as a function of matrix size (x-axis) and input noise precision (y-axis) for the difference of the two sides of Formula (6.3).

Basic Function	$e^{x \pm \delta x}$	$\log(x \pm \delta x)$	$(1 \pm \delta x)^c$	$\sin(x \pm \delta x)$
Range	$x \in [-100, +100]$	$x \in [1/32, 32]$	$c \in [-3, +3]$	$x \in [-\pi, +\pi]$
Error Deviation	$1.000 \pm 0.010$	$0.999 \pm 0.011$	$0.989 \pm 0.104$	$0.978 \pm 0.150$

Table 1: The result error deviation of selected basic functions using variance arithmetic when  $\delta x > 10^{-15}$ . The error deviation for  $(1 \pm \delta x)^c$  can be improved to  $0.998 \pm 0.034$  if diverge regions are excluded. The error deviation for  $\sin(x \pm \delta x)$  can be improved to  $1.000 \pm 0.010$  if pole regions are excluded.

Because an element of the original matrix  $\mathbf{M}$  appears multiple times in Formula (6.4), its result variance is very complicated using Formula (2.9). For example, Formula (6.5) shows the simplest case for Formula (6.4): the first-order approximation of a 2x2 matrix. Contrary to traditional approach, statistical Taylor expansion uses Formula (6.4) for matrix inversion instead of Gaussian elimination [5], because logically, the result should be symmetric for all matrix elements, as what Formula (6.5) has demonstrated.

In Formula (6.4),  $\mathbf{M}^{-1}$  is dominated by  $1/|\mathbf{M}|$ , suggesting that the precision of  $\mathbf{M}^{-1}$  is largely determined by the precision of  $|\mathbf{M}|$ . Figure 16 shows that there is a strong linear correlation between conditional numbers and the corresponding determinant precision of matrices. As a reference, Figure 16 presents the Hilbert matrix [20] for each matrix size and shows that the Hilbert matrices also follow the linear relation between determinant precision and condition number. Thus, determinant precision can replace matrix condition number.

## 7 Mathematical Library Functions

Table 1 shows that Formula (2.15), (2.17), (2.20), and (2.22) provide almost perfect deviation for the result values which are calculated using corresponding math library functions by sampling from  $x \pm \delta x$  in which  $\delta x$  is Gaussian input noise deviation. Table 1 shows the results from Python, which differs slightly from those from either C++ or Java.

The result error deviation is similar to Figure 14 but with the specific dimension as  $x$  in  $e^{x \pm \delta x}$  and  $\log(x \pm \delta x)$ , or  $c$  in  $(1 + \delta x)^c$ . The coverage is only proper when  $\delta x < 10^{-15}$ .

Figure 17 shows that the error deviation for  $\sin(x + \delta x)$  is  $1.000 \pm 0.010$ , except approaching 0 when  $x = \pm\pi/2$  and  $\delta x < 10^{-8}$ . Near a distributional pole, the input uncertainty is suppressed, resulting in zero error deviation. As expected,  $\delta^2 \sin(x)$  exhibits the same periodicity as  $\sin(x)$ . The numerical errors of the library functions  $\sin(x)$  and  $\cos(x)$  over a larger range of  $x$  will be examined in greater detail in Section 10.

To test  $f^{-1}(f(x)) - x = 0$  when  $\delta x = 0$  for the library functions:

- Figure 18 shows that the value errors in  $e^{\log(x)} - x$  are much less than those in  $\log(e^x) - x$ . For  $\log(e^x) - x$ , the error deviation is 0.41 when  $|x| \leq 1$ , or 0 otherwise.
- Figure 19 shows that the error deviation for  $(x^p)^{1/p} - x$  is 0.56, independent on neither  $x$  nor  $p$ .

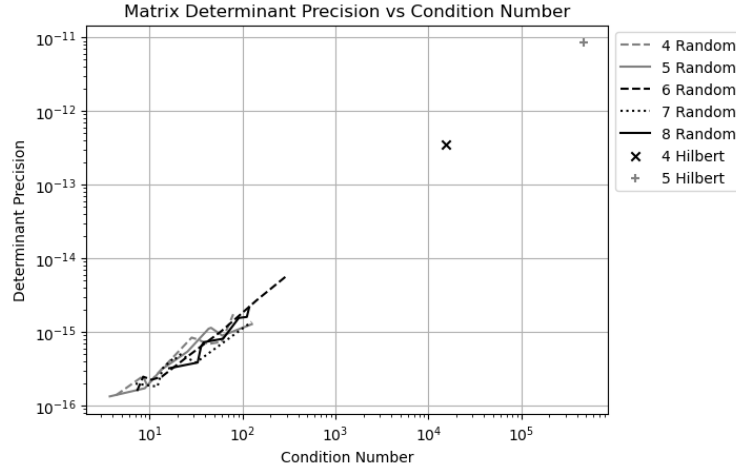


Figure 16: Linear correlation between the precision of a matrix determinant (y-axis) to its condition number (x-axis). The legend shows the size of the matrix, as well as the type of the matrix as *Random* for randomly generated matrix, and *Hilbert* as the Hilbert matrix.

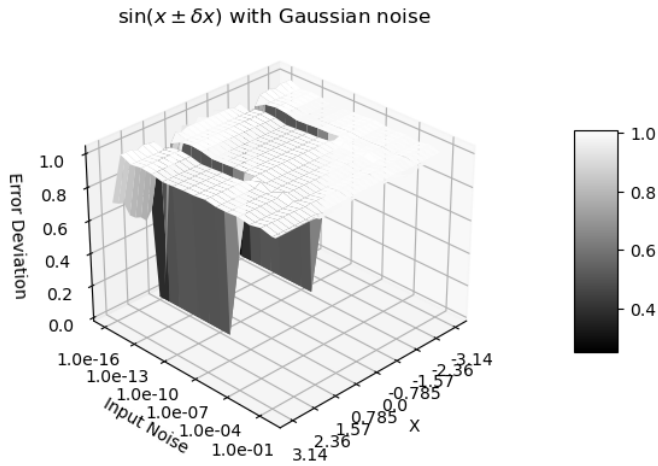


Figure 17: Error deviation for  $\sin(x \pm \delta x)$  as a function of  $x$  and  $\delta x$ . The x-axis represents  $x$  value between  $-\pi$  and  $+\pi$ . The y-axis represents  $\delta x$  value between  $-10^{-16}$  and 1. The z-axis shows the corresponding error deviation.

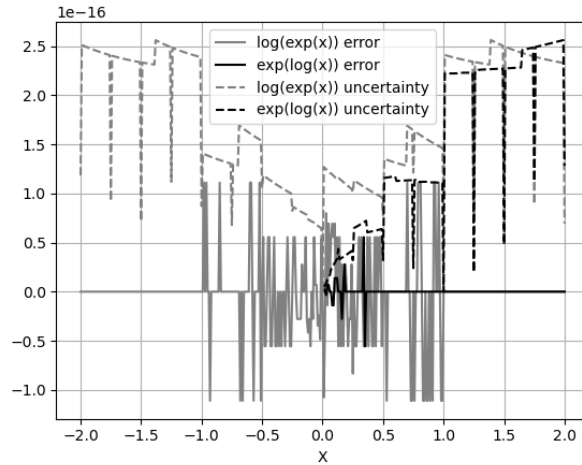


Figure 18: Values and uncertainties of  $\log(e^x) - x$  and  $e^{\log(x)} - x$  as functions of  $x$ , evaluated at 0.1 increment. When  $x$  is 2's fractional such as  $1/2$  or  $1$ , the result uncertainties are significantly smaller.

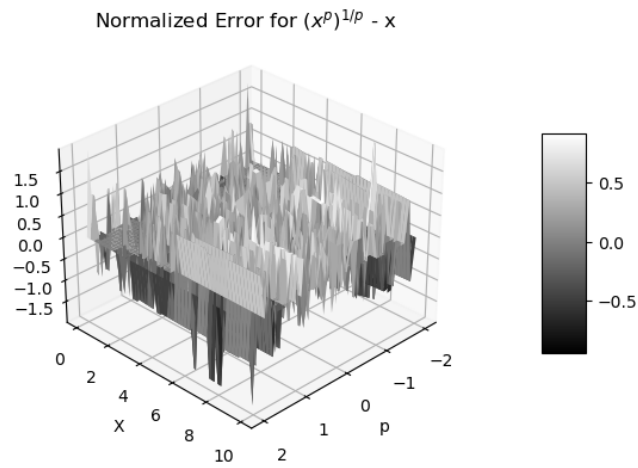


Figure 19: Normalized errors of  $(x^p)^{\frac{1}{p}} - x$  as functions of  $x$  and  $p$ .

The reasons why  $(x^p)^{1/p} - x$  has larger value errors than  $\log(e^x) - x$ , and  $e^{\log(x)} - x$  has almost no value error, are not clear.

## 8 Moving-Window Linear Regression

### 8.1 Moving-Window Linear Regression Algorithm

Formula (8.1) and (8.2) provide the least-square line-fit of  $Y = \alpha + \beta X$  between two set of data  $Y_j$  and  $X_j$ , where  $j$  is an integer index identifying  $(X, Y)$  pairs in the sets [5].

$$\alpha = \frac{\sum_j Y_j}{\sum_j 1}; \quad (8.1)$$

$$\beta = \frac{\sum_j X_j Y_j \sum_j 1 - \sum_j X_j \sum_j Y_j}{\sum_j X_j X_j \sum_j 1 - \sum_j X_j \sum_j X_j}; \quad (8.2)$$

In many applications, data set  $Y_j$  denotes an input data stream where  $j$  represents the time index or sequence index.  $Y_j$  is thus referred to as a time-series input, with  $j$  corresponding to  $X_j$ . A moving window algorithm [5] is applied within a small window centered on each  $j$ . For each calculation window,  $X_j = -H, -H + 1 \dots H - 1, H$  where  $H$  is an integer constant specifying the half width of the window. This choice ensures  $\sum_j X_j = 0$ , which simplifies Formula (8.1) and (8.2) into Formula (8.3) and (8.4), respectively [17].

$$\alpha_j = \alpha \ 2H = \sum_{X=-H+1}^H Y_{j-H+X}; \quad (8.3)$$

$$\beta_j = \beta \frac{H(H+1)(2H+1)}{3} = \sum_{X=-H}^H XY_{j-H+X}; \quad (8.4)$$

The values of  $(\alpha_j, \beta_j)$  can be derived from the previous values  $(\alpha_{j-1}, \beta_{j-1})$ , allowing Formula (8.3) and (8.4) to be reformulated into the progressive moving-window calculation given by Formula (8.5) and (8.6), respectively [17].

$$\beta_j = \beta_{j-1} - \alpha_{j-1} + H(Y_{j-2H-1} + Y_j); \quad (8.5)$$

$$\alpha_j = \alpha_{j-1} - Y_{j-2H-1} + Y_j; \quad (8.6)$$

### 8.2 Variance Adjustment

$$\delta^2 \alpha_j = \sum_{X=-H+1}^H (\delta Y_{j-H+X})^2 = \delta^2 \alpha_{j-1} - (\delta Y_{j-2H})^2 + (\delta Y_j)^2; \quad (8.7)$$

$$\delta^2 \beta_j = \sum_{X=-H}^H X^2 (\delta Y_{j-H+X})^2; \quad (8.8)$$

When the time series contains uncertainty, directly applying Formula (8.5) and (8.6) results in a loss of precision since both formulas reuse each input multiple times,

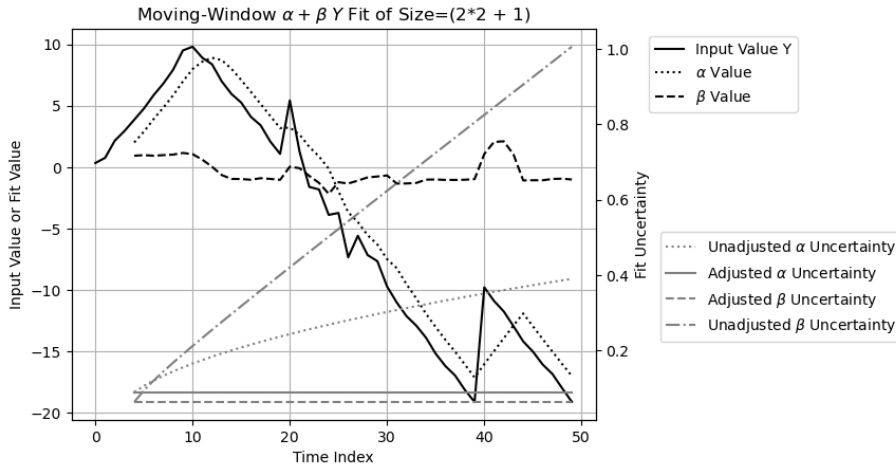


Figure 20: Result of fitting  $\alpha + \beta Y$  to a time-series input  $Y$  within a moving window of size  $2 * 2 + 1$ . The x-axis indicates the time index. The y-axis on the left corresponds to the value of  $Y$ ,  $\alpha$ , and  $\beta$ , while the y-axis on the right corresponds to the uncertainty of  $\alpha$  and  $\beta$ . The uncertainty for  $Y$  is fixed at 0.2. In the legend, *Unadjusted* refers to results obtained by directly applying Formula (8.5) and (8.6) using variance arithmetic, whereas *Adjusted* refers to using Formula (8.5) and (8.6) for  $\alpha$  and  $\beta$  values but Formula (8.7) and (8.8) for their variances.

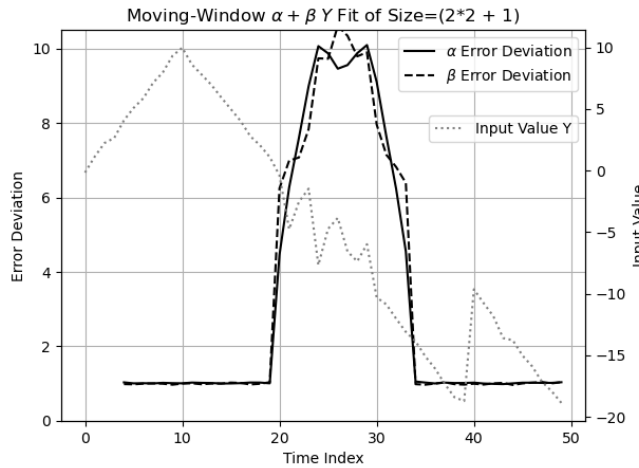


Figure 21: Error deviations of the  $\alpha + \beta Y$  fit vs time index. The x-axis represents the time index. The y-axis on the left corresponds to the error deviation. For reference, the input time-series signal  $Y$  is also plotted, with its values indicated on the y-axis on the right.

thereby accumulating the variance of that input with every reuse. To prevent this,  $\alpha_j$  and  $\beta_j$  should still be calculated progressively using Formula (8.6) and (8.5), respectively, while the variances should instead be computed using Formula (8.7) and (8.8), respectively. Formula (8.8) is not progressive because the progressive form of  $\delta^2\beta_j$  is more expensive in computation than Formula (8.8).

Figure 20 shows that the input signal  $Y_j$  consists of the following components:

1. An increasing slope for  $j = 0 \dots 9$ .
2. A decreasing slope for  $j = 1 \dots 39$ .
3. A sudden jump of magnitude +10 at  $j = 40$ .
4. A decreasing slope for  $j = 41 \dots 49$ .

For each increment of  $j$ , the increasing and the decreasing rates are +1 and -1, respectively.

The specified input uncertainty is fixed at 0.2. Normal noise with a deviation of 0.2 is added to the slopes, except for the segment  $j = 10 \dots 19$  where Normal noise with a deviation of 2 is introduced, representing actual uncertainty 10 times larger than the specified uncertainty.

Figure 20 also presents the results of the moving window fitting of  $\alpha + \beta Y$  versus the time index  $j$ . The fitted values of  $\alpha$  and  $\beta$  follow the expected behavior, exhibiting a characteristic delay of  $H$  in  $j$ . When (8.3) and (8.4) are applied to compute the uncertainties of  $\alpha$  and  $\beta$ , both uncertainties increase exponentially with the time index  $j$ . In contrast, when Formula (8.3) and (8.4) are used exclusively for value calculation, while Formula (8.7) and (8.8) are applied for variance computation, the resulting uncertainties of  $\alpha$  and  $\beta$  are  $\frac{\delta Y}{\sqrt{2H+1}}$ , and  $\frac{\delta Y}{\sqrt{\frac{H(H+1)(2H+1)}{3}}}$ . Both are less than the input uncertainty  $\delta Y$ , due to the averaging effect of the moving window.

### 8.3 Unspecified Input Error

To determine the error deviations of  $\alpha$  and  $\beta$ , the fitting procedure is applied to multiple time-series data sets, each generated with independent noise realizations. Figure 21 illustrates the resulting error deviation as a function of the time index  $j$ , which remains close to 1 except within the range  $j = 10 \dots 19$  where the actual noise is ten times greater than the specified value. This observation suggests that an error deviation exceeding 1 may indicate the presence of unspecified additional input errors beyond rounding errors, such as numerical errors in mathematical library functions.

## 9 Regressive Generation of Sin and Cos

Formula (9.2) and Formula (9.3) calculate  $\sin(\pi j/2^L)$ ,  $\cos(\pi j/2^L)$ ,  $j = 0 \dots 2^{L-2}$  progressively for regression order  $L = 0 \dots 17$  starting from Formula (9.1). Formula (9.4) shows that such regression guarantees both  $\sin(x)^2 + \cos(x)^2 = 1$  and  $\sin(2x) = 2\sin(x)\cos(x)$ , so that value errors will not accumulate when the regression order

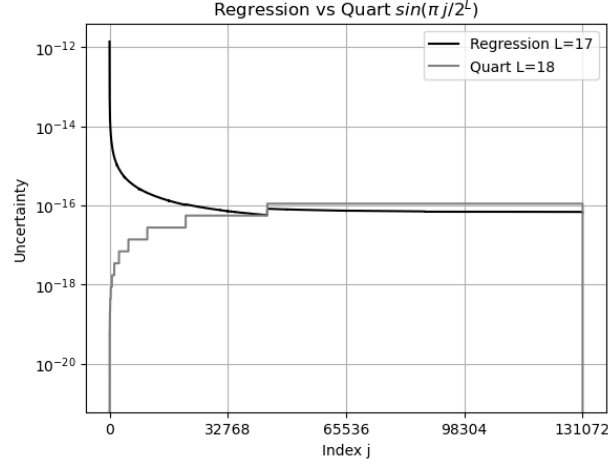


Figure 22: The uncertainties (y-axis) of  $\sin(\pi j/2^{18})$  versus  $j$  (x-axis) and  $L$  using either Quart or regressive sine function (legend).

increases.

$$\sin(0) = \cos\left(\frac{\pi}{2}\right) = 0; \quad \sin\left(\frac{\pi}{2}\right) = \cos(0) = 1; \quad (9.1)$$

$$\sin\left(\frac{\alpha + \beta}{2}\right) = \sqrt{\frac{1 - \cos(\alpha + \beta)}{2}} = \sqrt{\frac{1 - \cos(\alpha)\cos(\beta) + \sin(\alpha)\sin(\beta)}{2}}; \quad (9.2)$$

$$\cos\left(\frac{\alpha + \beta}{2}\right) = \sqrt{\frac{1 + \cos(\alpha + \beta)}{2}} = \sqrt{\frac{1 + \cos(\alpha)\cos(\beta) - \sin(\alpha)\sin(\beta)}{2}}; \quad (9.3)$$

$$\sin(\alpha + \beta) = 2 \sin\left(\frac{\alpha + \beta}{2}\right) \cos\left(\frac{\alpha + \beta}{2}\right) = \sqrt{1 - \cos\left(\frac{\alpha + \beta}{2}\right)^2}; \quad (9.4)$$

Formula (9.2) is not suitable for computing  $\sin(x)$  as  $x \rightarrow 0$  because it suffers from behavior analogous to catastrophic cancellation, resulting in excessive uncertainty. In Figure 22, the Quart sine function exhibits uncertainties proportional to  $\sin(\frac{\pi}{2^L})$ , whereas the regression sine function shows increasing uncertainties as  $x \rightarrow 0$ . Unlike catastrophic cancellation in floating-point arithmetic, variance arithmetic uses very coarse precision to signal that the regression algorithm is unfit to compute  $\sin(x \rightarrow 0)$ .

## 10 FFT (Fast Fourier Transformation)

### 10.1 DFT (Discrete Fourier Transformation)

$$H[n] = \sum_{k=0}^{N-1} h[k] e^{\frac{i2\pi}{N}kn}; \quad (10.1)$$

$$h[k] = \frac{1}{N} \sum_{n=0}^{N-1} H[n] e^{-\frac{i2\pi}{N}nk}; \quad (10.2)$$

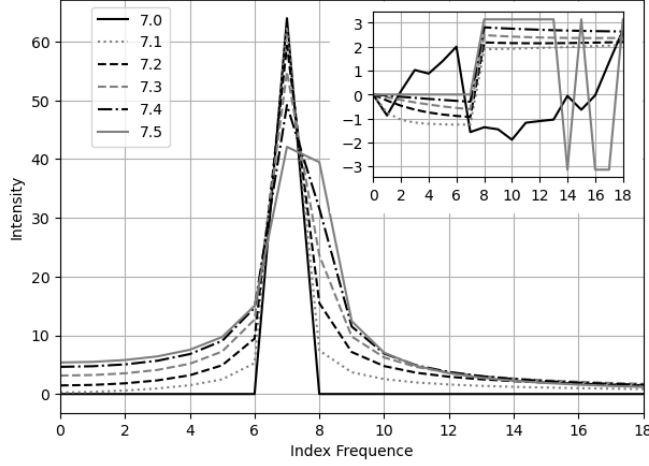


Figure 23: The DFT spectrum  $H[n]$  of signal  $h[k] = \sin(f \frac{2\pi}{128} k)$ ,  $k \in [0, 127]$ , as intensity (y-axis) and phase (embedded y-axis) versus frequency index  $n \in [0, 18]$  (x-axis and embedded x-axis) for different signal frequency  $f$  (legend). This result agrees with both theoretical formula [17] and numerical computation from any mathematical libraries such as *SciPy*.

For each signal sequence  $h[k]$ , where  $k = 0, 1 \dots N - 1$ , and  $N$  is a natural number, the discrete Fourier transform (DFT)  $H[n]$ , for  $n = 0, 1 \dots N - 1$ , along with its inverse transformation, is defined by Formula (10.1) and (10.2), respectively [5]. As a convention,  $k$  denotes *time index* for  $h[k]$  as a waveform, while  $n$  represents *frequency index* for  $H[n]$  as a spectrum.

For example, the FT spectrum of a sine function is a Delta function at the signal frequency  $f$  with a phase  $\pi/2$  [5]. Figure 23 shows the DFT spectra of the sine function  $h[k] = \sin(f \frac{2\pi}{128} k)$ ,  $k \in [0, 127]$ , where  $f$  is its signal frequency. If DFT is regarded as the digital implementation of FT, the spectra exhibit no modeling error only when the input signal frequency  $f$  is an integer, and display varying degrees of modeling errors otherwise. Because of these modeling errors, the use of DFT as the digital implementation of FT is questionable, even though such usage is ubiquitous, and fundamental to many areas of applied mathematics

To avoid the modeling errors inherent in DFT, only Formula (10.1) and (10.2) are used in this paper.

## 10.2 FFT (Fast Fourier Transformation)

When  $N = 2^L$ , where  $L$  is a natural number named *FFT order*, the generalized Danielson-Lanczos lemma can be applied to DFT to produce FFT [5].

- For each output, each input is used only once, therefore no dependency problem arises when decomposing FFT into arithmetic operations such as Formula (2.10), (2.11), (2.12), and (2.13).
- When  $L$  is large, the substantial volume of input and output data enables high-quality statistical analysis.

- The computational complexity is proportional to  $L$ , since increasing  $L$  by 1 adds an additional step involving a sum of two multiplications.
- Each step in the forward transformation doubles the variance, so the uncertainty deviation increases with the FFT order  $L$  as  $\sqrt{2}^L$ . Because the reverse transformation divides the result by  $2^L$ , its uncertainty deviation decreases with  $L$  as  $\sqrt{1/2}^L$ . Consequently, the uncertainty deviation for the roundtrip transformation is therefore  $\sqrt{2}^L \times \sqrt{1/2}^L = 1$ .
- The forward and reverse transformations are identical except for a sign difference, meaning that they are essentially the same algorithm, and any observed difference arises solely from the input data.

In normal usage, forward and reverse FFT transforms differ in their data prospective of time domain versus frequency domain:

- The forward transformation converts a time-domain sine or cosine signal into a frequency-domain spectrum in which most values are zero, causing its uncertainties to grow more rapidly by cancellation.
- In contrast, the reverse transformation spreads the precise frequency-domain spectrum (where most values are zero) back into a time-domain sine or cosine signal, causing its uncertainties to grow more slowly by spreading.

The question is whether variance arithmetic can work properly in these two contrary cases.

### 10.3 Testing Signals

The following signals are used for testing:

- *Sin*:  $h[k] = \sin(2\pi k f/N)$ ,  $f = 1, 2, \dots, N/2 - 1$ .
- *Cos*:  $h[k] = \cos(2\pi k f/N)$ ,  $f = 1, 2, \dots, N/2 - 1$ .
- *Linear*:  $h[k] = k$ , whose DFT is given by Formula (10.3).

$$y \equiv i2\pi \frac{n}{N} : G(y) = \sum_{k=0}^{N-1} e^{yk} = \frac{e^{Ny} - 1}{e^y - 1};$$

$$H[n] = \frac{dG}{dy} = \begin{cases} n = 0 : & \frac{N(N-1)}{2} \\ n \neq 0 : & -\frac{N}{2} \left(1 + i \frac{\cos(n \frac{\pi}{N})}{\sin(n \frac{\pi}{N})}\right) \end{cases} ; \quad (10.3)$$

### 10.4 Trigonometric Library Errors

Formula (10.1) and (10.2) restrict the use of  $\sin(x)$  and  $\cos(x)$  to  $x = 2\pi j/2^L$ , where  $L$  is the FFT order. To minimize numerical errors in computing  $\sin(x)$ , the following *indexed sine* can be used in place of standard library sine functions:

1. Instead of a floating-point value  $x$  as input for  $\sin(x)$ , an integer index  $j$  defines the input as  $\sin(\pi j/2^L)$ , thereby eliminating the floating-point rounding error of  $x$ .
2. The values of  $\sin(\pi j/2^L)$ ,  $j \in [0, 2^{L-2}]$  are library sine directly, while the values of  $\sin(\pi j/2^L)$ ,  $j \in [2^{L-2}, 2^{L-1}]$  are computed from library  $\cos(\pi(2^{L-1} - j)/2^L)$ .
3. The values of  $\sin(\pi j/2^L)$  are extended from  $j \in [0, 2^{L-1}]$  to  $j \in [0, 2^{L+1}]$  by exploiting the symmetry of  $\sin(\pi j/2^L)$ .

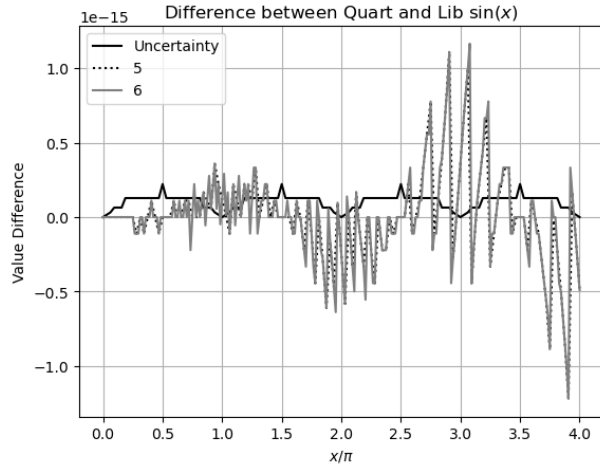


Figure 24: Difference between library and Quart  $\sin(x)$  (y-axis) for  $x = 2\pi j/2^L, j = 0, 1 \dots 2^{L+2}$  (x-axis), and  $L = 5, 6$  (legend). The uncertainties of the Quart  $\sin(x)$  is  $\sin(x)$  ULP, which shows a periodicity of  $\pi$ .

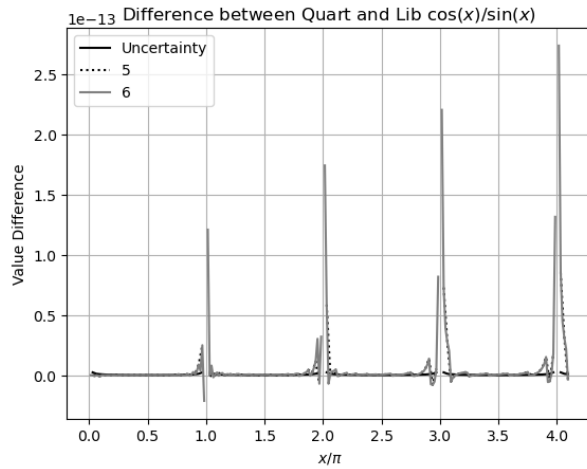


Figure 25: Difference between the library and the Quart  $\cos(x)/\sin(x)$  (y-axis) for  $x = 2\pi j/2^L, j = 0, 1 \dots 2^{L+2}$  (x-axis), and  $L = 5, 6$  (legend).

4. The values of  $\sin(\pi j/2^L)$  are extended to all the integer value of  $j$  by leveraging the periodicity of  $\sin(2\pi j/2^L)$ .

The constructed indexed  $\sin(x)$  is referred to as the *Quart* sine function. In contrast, the direct use of the standard library  $\sin(x)$  is referred to as the *Library* sine function.

Because the Quart sine function strictly preserves the symmetry and periodicity of sine function, it provides superior numerical accuracy compared to the Library sine function.

- Figure 24 shows that the absolute value difference between the Library  $\sin(x)$  and the Quart  $\sin(x)$  increases approximately linearly with  $|x|$ .
- Figure 25 shows the value difference between the Quart and Library  $\cos(x)/\sin(x)$  also increases roughly linearly with  $|x|$  but are  $10^2$  times larger than those observed for  $\sin(x)$ . Therefore, the linear spectrum in Formula (10.3) contains significantly larger numerical errors when computed using library sine functions.

## 10.5 Using Quart Sine for Sin/Cos Signals

With FFT order as the specific dimension, the error deviations for forward and reverse transformations resemble Figure 14, while those for round-trip transformation is almost identical to Figure 15, independent of Sin or Cos signals, or frequency of the signals. Therefore, the results for Sin and Cos signals across all frequencies are pooled together for statistical analysis, under the unified category *Sin/Cos* signals. When the FFT order  $L$  is less than 8, the error deviations oscillate around 1 due to insufficient sample count of  $2^L$ . Even data for forward and reverse transformations are drastically different, variance arithmetic works effectively in all cases.

When  $L = 18$  and  $\delta x = 0$ , Figure 26 shows that the error distributions of Sin/Cos signal resemble Normal distribution, with an additional Delta-like distribution at  $\tilde{z} = 0$ . The error distribution of the reverse transformation is structured on top of the Normal distribution, suggesting that the reverse transformation is more sensitive to numerical errors in sine function.

## 10.6 Using Library Sine for Sin/Cos Signals

With FFT order as the specific dimension, the error deviations for the forward and the reverse transformations resemble Figure 14, while those for the round-trip transformation is almost identical to Figure 15. In addition, the error deviations are larger than 1 when  $\delta x < 10^{-15}$  for the forward transformation and  $\delta x < 10^{-14}$  for the reverse transformation.

When  $\delta x = 0$ , the error deviations for the reverse transformation increase with FFT order, to 6.2 at FFT order 18. As shown in Figure 24, the Library sine function contains more numerical errors, so the error distribution for the reverse transformation using Library sine function in Figure 27 is more structured and broader than that in Figure 26 using Quart sine function, while the error distribution for the forward transformations is more similar. This difference is consistent with a larger error deviation  $6.2 > 1$  for the reverse transformation, but a comparable error deviation  $1.1 > 1$  for the forward transformation when  $\delta x = 0$ .

Using the Library sine function, for a sine wave with a frequency of 3, Figure 28, 29, and 30 presents the value errors for the forward, the reverse, and the round-trip transformations, respectively. In the reverse transformation, value errors exhibit a

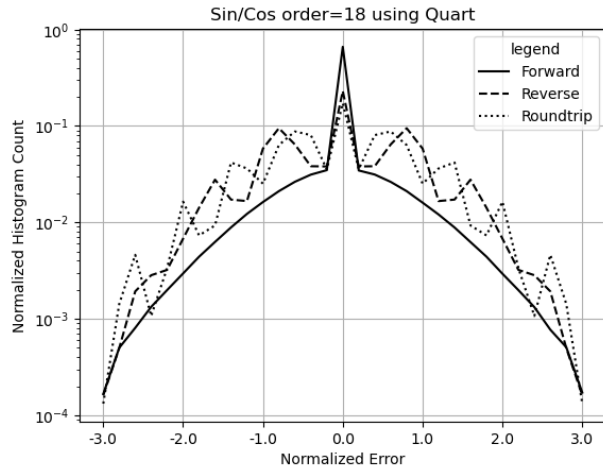


Figure 26: Histograms of normalized errors of Sin/Cos signals for forward, reverse and roundtrip transformations (legend) using the Quart sine function. The FFT order is 18.

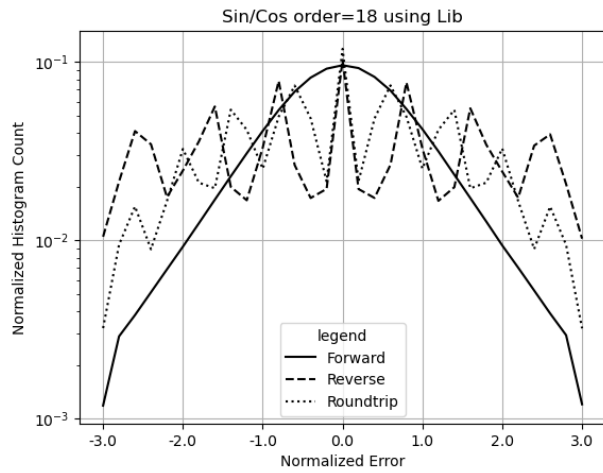


Figure 27: Histograms of normalized errors of Sin/Cos signal for forward, reverse and roundtrip transformations (legend) computed using the Library sine function. The FFT order is 18.

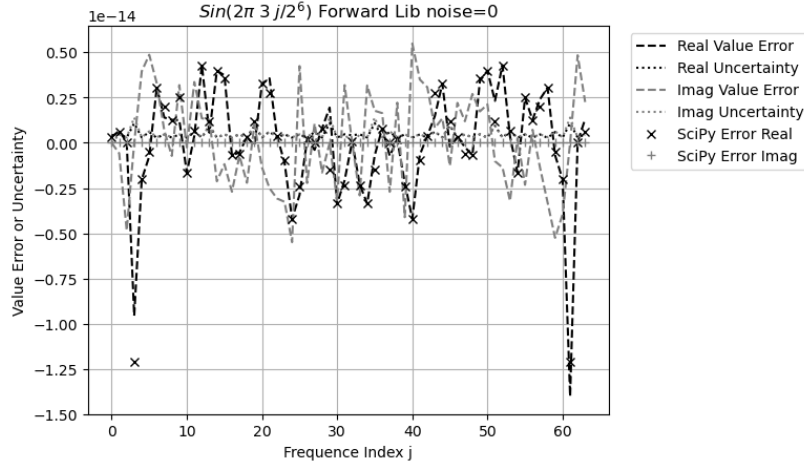


Figure 28: FFT value error spectrum of  $\sin(3\frac{2\pi}{2^6}j)$  computed using either the Library sine function or *SciPy* after the forward transformation. The legend distinguishes between uncertainty and value error. The x-axis represents the frequency index, while the y-axis represents both uncertainty and value error.

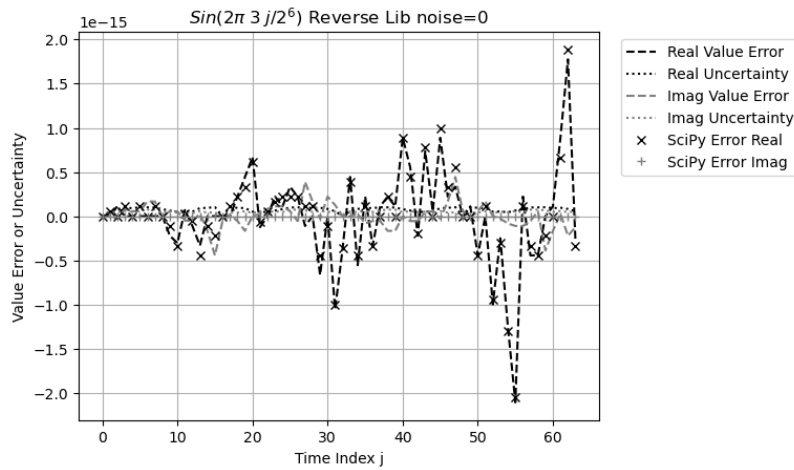


Figure 29: FFT value error waveform of  $\sin(3\frac{2\pi}{2^6}j)$  computed using either the Library sine function or *SciPy* after the reverse transformation. The legend distinguishes between uncertainty and value error. The x-axis represents the time index, while the y-axis represents both uncertainty and value error.

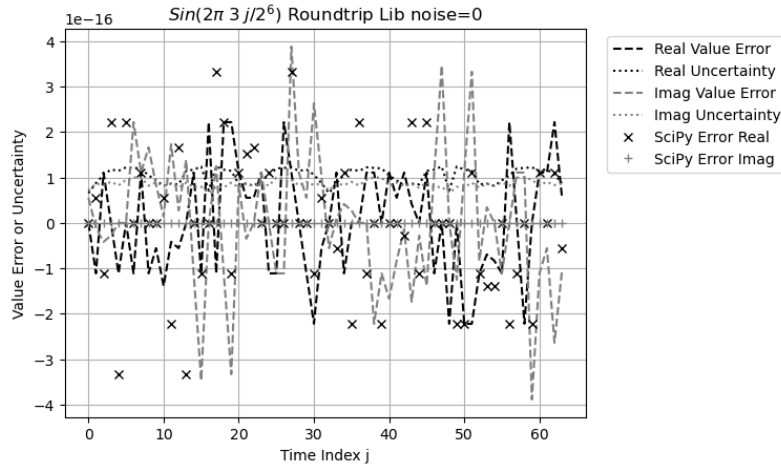


Figure 30: FFT value error waveform of  $\sin(3\frac{2\pi}{2^6}j)$  computed using either the Library sine function or *SciPy* after the roundtrip transformation. The legend distinguishes between the uncertainty and the value error. The x-axis represents the frequency index, while the y-axis represents both uncertainty and value error.

Sin Reverse noise=0 using Library sine

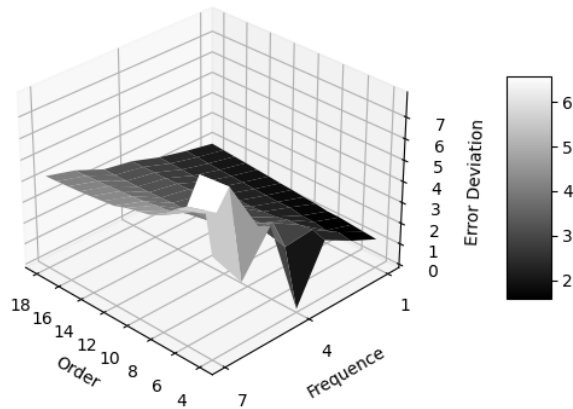


Figure 31: Error deviation (z-axis) of FFT reverse transformation of  $\sin(f\frac{2\pi}{2^L}j)$  versus frequency  $f$  (x-axis) and FFT Order  $L$  (y-axis).

clear trend of increasing with the time index. These large value errors appear systematic rather than random and visually resemble a resonant pattern. Similar increases are observed at other frequencies and FFT orders, as well as in computational results obtained using mathematical libraries such as *SciPy*. In contrast, such resonance is absent for the roundtrip transformation as shown in Figure 30, as well as when using the Quart sine function. Figure 31 demonstrates that the error deviations increase with sine or cosine frequency. Figure 24 indicates that the numerical errors using the Library sine function increase with a periodicity of  $\pi$ , which may resonate with a signal whose periodicity is an integer multiply of  $\pi$ , producing the resonant pattern in Figure 29. At higher frequency, the resonant beats between the signal and the numerical errors in the Library sine function become stronger. To suppress these numerical error resonances, an input noise of  $\delta x = 10^{-14}$  must be added to the sine or cosine signals. Such *resonance of numerical errors* can easily and mistakenly be taken as signals.

## 10.7 Using Quart Sine for Linear Signal

Figure 32 and 33 show the error deviation for the forward and the reverse transformations, respectively. The forward transformation exhibits a larger ideal coverage area than the reverse transformations:  $\delta x > 10^{-12}$  for the forward transformation, and  $\delta x > 10^{-8}$  for the reverse transformation. In other areas, both transformations achieve proper coverage with error values around 1.

When  $L = 18$  and  $\delta x = 0$ , the error distribution of the reverse transformation in Figure 34 is narrower than that in Figure 27. The corresponding error deviations are  $1.5 < 6.2$ , respectively.

## 10.8 Using Library Sine for Linear Signal

Figure 35 shows that the reverse error distribution when  $\delta x = 0$  is no longer bound. The difference between Figure 35 and Figure 34 is consistent with the large numerical errors as demonstrated in Figure 25. Variance arithmetic fails because of the large amount of unspecified numerical errors from the Library sine.

Figure 36 and 37 shows a much smaller ideal coverage areas than those in Figure 32 and 33. Because result deviations grow more slowly in the reverse transformation than in the forward transformation, the reverse transformation exhibits a smaller ideal coverage region. Outside the ideal coverage region, proper coverage cannot be achieved for the reverse transformation. Furthermore, the range of input noise that produces ideal coverage decreases with increasing FFT order. At sufficiently high FFT orders, visually beyond FFT order 25 for the reverse transformation, ideal coverage may no longer be achievable. Although FFT is widely regarded as one of the most robust numerical algorithms [5][10], and generally insensitive to input errors, it can still fail due to numerical errors in the Library sine function. Such deterioration in calculation accuracy is not easily detectable when using conventional floating-point arithmetic.

Figure 38 shows that, even when variance arithmetic can no longer effectively track the value errors for the forward and the reverse transformations, it can still effectively track the value errors for the round-trip transformation, as the plateau region at high  $L$  and low  $\delta x$  in Figure 38. Such error cancellation is due to dependence tracing in statistical Taylor expansion.

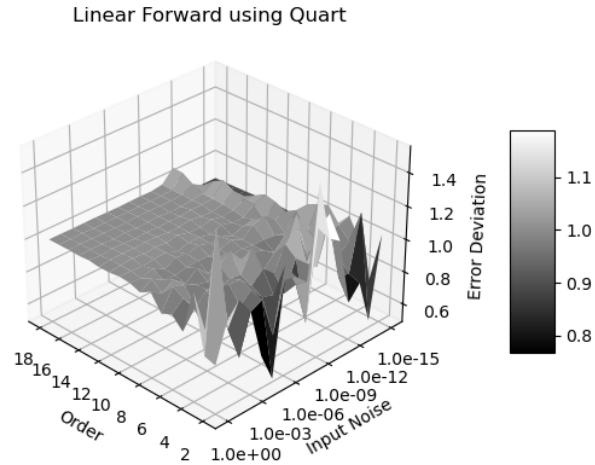


Figure 32: Error deviation (z-axis) versus input uncertainty (x-axis) and FFT order (y-axis) for the forward transformations of Linear signals computed using the Quart sine function.

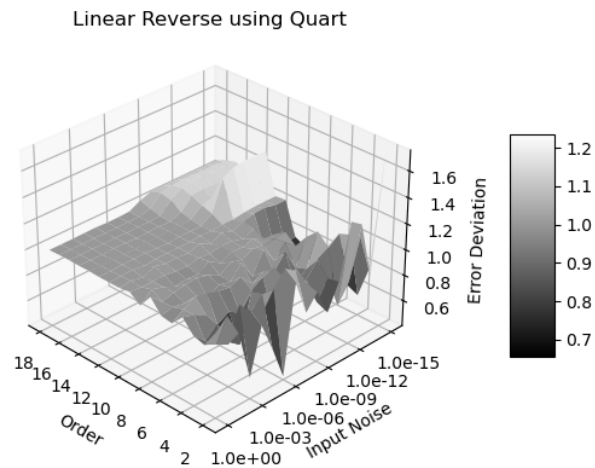


Figure 33: Error deviation (z-axis) versus input uncertainty (x-axis) and FFT order (y-axis) for the reverse transformations of Linear signals computed using the Quart sine function.

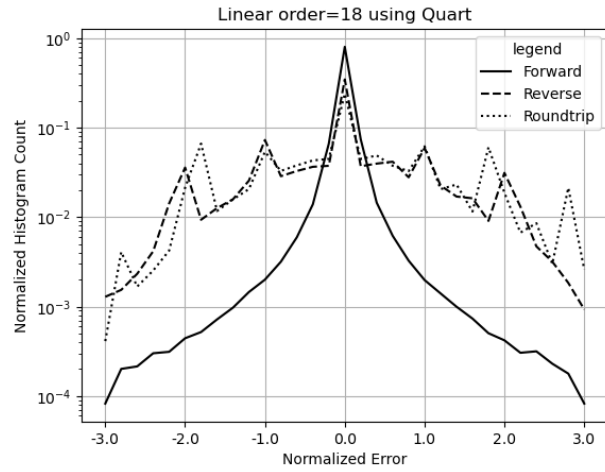


Figure 34: Histograms of normalized errors of Linear signals for forward, reverse and roundtrip transformations (legend) computed using the Quart sine function. The FFT order is 18.

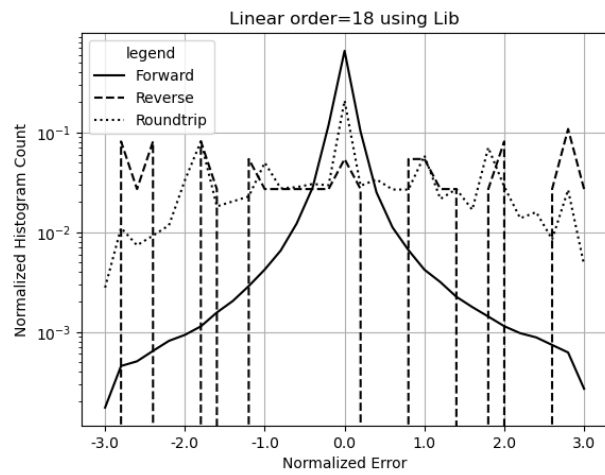


Figure 35: Histograms of normalized errors of Linear signals for forward, reverse and roundtrip transformations (legend) computed using the Library sine function. The FFT order is 18.

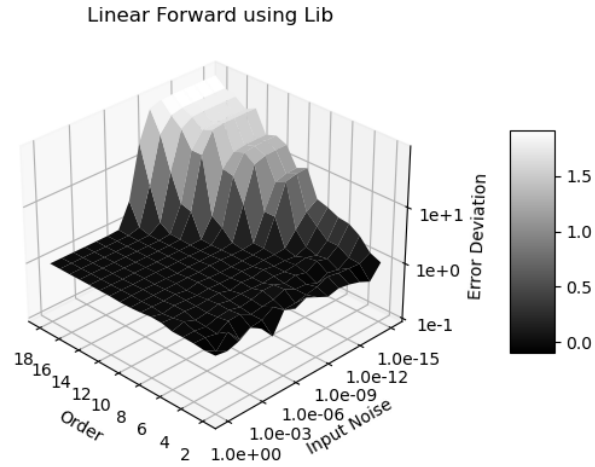


Figure 36: Error deviation (z-axis) versus input uncertainty (x-axis) and FFT order (y-axis) for the forward transformations of Linear signals computed using the Library sine function.

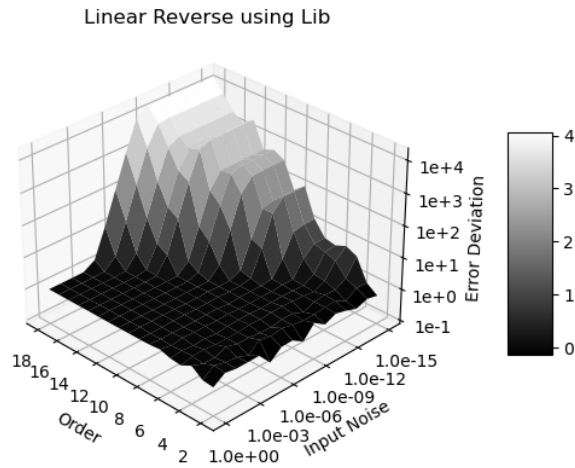


Figure 37: Error deviation (z-axis) versus input uncertainty (x-axis) and FFT order (y-axis) for the reverse transformations of Linear signals computed using the Library sine function.

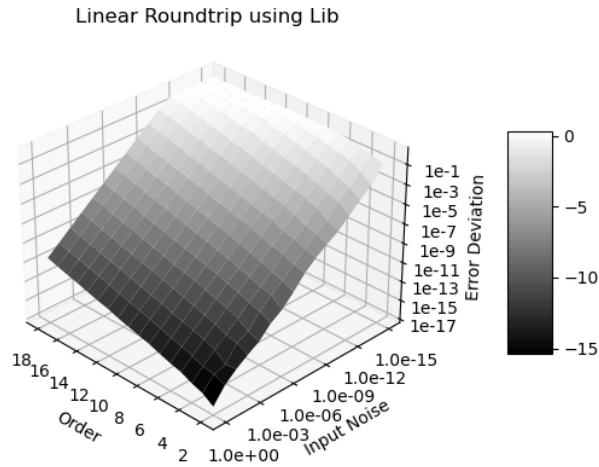


Figure 38: Error deviation (z-axis) versus input uncertainty (x-axis) and FFT order (y-axis) for the roundtrip transformations of Linear signals computed using the Library sine function.

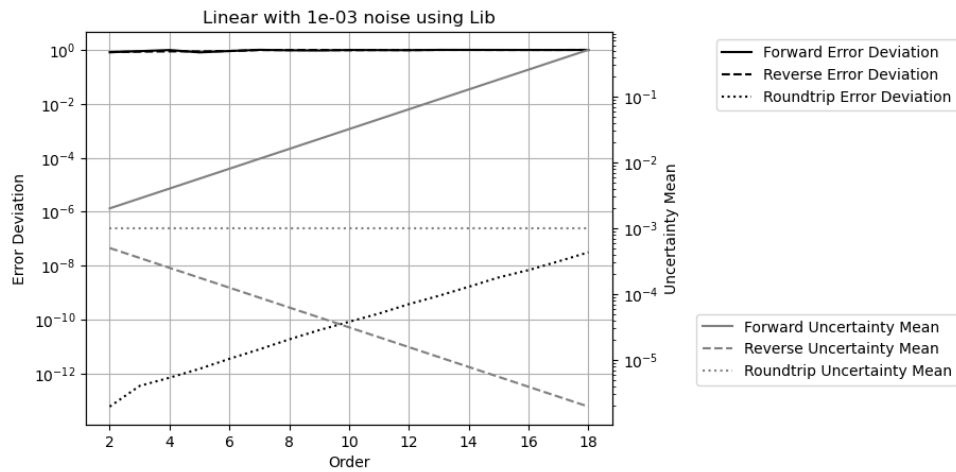


Figure 39: Result error deviation (left y-axis) and uncertainty deviation (right y-axis) of Linear signals versus FFT order (x-axis) and transformation types (legend) computed using the Library sine function.

Signal	Sine function	Forward	Reverse	Roundtrip
Sin/Cos	Quart	$10^{-16}$	$10^{-12}$	$10^{-14}$
Sin/Cos	Library	$10^{-16}$	$10^{-11}$	$10^{-12}$
Linear	Quart	$10^{-11}$	$10^{-7}$	$10^{-8}$
Linear	Library	$10^{-11}$	$10^{-3}$	$10^{-8}$

Table 2: The measured minimal required noise to achieve ideal coverage for FFT transformations at FFT order 18 for different signals and sine functions.

## 10.9 Ideal Coverage

Adding noise to the input can suppress unspecified input errors. After adding a Gaussian input noise of  $\delta x = 10^{-3}$  to a Linear signal when using the Library sine function, the error distributions for both the forward and the reverse transformations become Normal, while the error distribution for the round-trip transformation becomes Delta. Figure 39 illustrates the corresponding error deviations and uncertainty deviations versus FFT order:

- As expected, the resulting uncertainty deviations for the forward transformations increase with FFT order  $L$  as  $\sqrt{2}^L$ .
- As expected, the resulting uncertainty deviations for the reverse transformations decrease with FFT order  $L$  as  $1/\sqrt{2}^L$ .
- As expected, the resulting uncertainty deviations for the round-trip transformations remains equal to the corresponding input uncertainties of  $10^{-3}$ .
- As expected, the resulting error deviations for the forward and the reverse transformations remain constant at 1.
- As expected, the resulting error deviations for the round-trip transformations are far less than 1 but increase with FFT order  $L$  exponentially due to increasing calculation.

Table 2 shows the minimal required noise to achieve ideal coverage for FFT transformations at FFT order  $L = 18$  for different signals and sine functions, which is consistent with the corresponding error distributions in Figure 26, 27, 34, and 35. This shows that an error distribution can qualify its input uncertainty quantification. Without knowing precise result, similar histogram can be constructed from the calculated mean  $\bar{f}$  and deviation  $\delta f$ , and the result data set for  $f$ . It is worth investigating if such empirical histogram has similar power to reveal tracking of value errors by variance arithmetic.

# 11 Conclusion and Discussion

## 11.1 Summary

When uncorrelated uncertainty condition is met, statistical Taylor expansion outputs the mean, deviation, and reliability of an analytic expression. It tracks the variable dependencies in intermediate steps, rejects invalid calculations, and explicitly incorporates the sample counts and the input uncertainty distributions into the statistical

analysis. While statistical Taylor expansion eliminates the dependency problem, it also removes most execution flexibility.

The presence of ideal coverage is a necessary condition for a numerical algorithm using statistical Taylor expansion to be considered correct. The ideal coverage defines the optimal applicable range for an algorithm.

Variance arithmetic simplifies statistical Taylor expansion by introducing numerical rules to elimination invalid results, such as divergent, negative variance, unstable, infinite, or unreliable results. It provides proper coverage for floating-point rounding errors. The applicability of variance arithmetic has been demonstrated across a wide range of computational scenarios.

Library mathematical functions should be recalculated using variance arithmetic, so that each output value is accompanied by its corresponding uncertainty. Without this refinement, the value errors in the library functions can produce unpredictable and potentially significant effects on numerical results.

The code and analysis framework for variance arithmetic are available as an open-source project at <https://github.com/Chengpu0707/VarianceArithmetic>. A more detailed description of this paper is presented at <https://arxiv.org/abs/2410.01223>.

## 11.2 Improvements Needed

This paper presents statistical Taylor expansion and variance arithmetic, which is still in early stage of development, with several important questions remaining.

Bound momentum  $\zeta(2n)$  needs to be extended to all probability distributions. The statistical bounding to find the bounding range  $\kappa$  for a sample count needs to be extended to discrete distributions. The choice of ideal bounding range  $\hat{\kappa}$  needs to extend to other distributions. The statistical meaning for ideal ratio  $\alpha$  in the context of its choice of ideal bounding range  $\hat{\kappa}$  needs further investigation: Is  $\alpha$  the possibility for the result to be bound by  $\hat{\kappa}$ ?

The performance of variance arithmetic must be improved for broader practical adoption. The fundamental formulas of statistical Taylor expansion, Formula (2.5), (2.6), (2.8), and (2.9), contain a large number of independent summations, making them excellent candidates for parallel processing. Moreover, the inherently procedural nature of these formulas allows statistical Taylor expansion to be implemented efficiently at the hardware level.

A key open question is whether variance arithmetic can be adapted to achieve ideal coverage for floating-point rounding errors, because many theoretical calculations lack explicit input uncertainties. Variance arithmetic does not adjust uncertainty variance when floating-point rounding error occurs during calculation. This leads to error deviations larger than 1. Detecting floating-point rounding error also needs hardware implementation for efficiency.

In variance arithmetic, deviations are comparable with values, but variances are used in calculation. This effectively limits the range of deviations to the square root of that of values. If the sign bit of the floating type can be re-purposed as an exponent bit in a new unsigned floating-point representation, the range of the deviation will be identical to that of values.

When an analytic expression undergoes statistical Taylor expansion, the resulting expression can become highly complex, as in the case of matrix inversion. However, modern symbolic computation tools such as *SymPy* and *Mathematica* can greatly facilitate these calculations. This observation suggests that it may be time to shift

from purely numerical programming toward analytic programming, particularly for problems that possess inherently analytic formulations.

As an enhancement to dependency tracing, source tracing identifies each input's contribution to the overall result uncertainty. This capability enables engineers to pinpoint the primary sources of measurement inaccuracy and in turn guide targeted improvements in data acquisition and processing strategies. For example, Formula (2.31) can guide how to improve the ideal ratio of  $x \pm y$ .

Because traditional numerical approaches are based on floating-point arithmetic, they must be reexamined or even reinvented within the framework of variance arithmetic. For instance, most conventional numerical algorithms aim to identify optimal computational paths, whereas statistical Taylor expansion conceptually rejects all path-dependent calculations. Reconciling these two paradigms may present a significant and ongoing challenge.

Establishing theoretical foundation for applying statistical Taylor expansion in the absence of a closed-form analytic solution, or when only limited low-order numerical derivatives are available, as in solving differential equations, remains an important direction for future research.

### 11.3 Possible Connections to Quantum Physics

For input distribution without bounding, Formula (2.6) may not converge, for example, when the input uncertainty is Laplace [4] so that  $\zeta(2n) = (2n)!$ . Formula (2.6) converges in all cases only when the input uncertainty is bounded due to sampling, which resembles the need for re-normalization in quantum field theory [21]. The quantitative dependence of convergence on the choice of ideal bounding range  $\hat{\kappa}$  is similar to the principle of quantum physics: what it is depends on how it is measured. For example, because mathematical divergence seems to correspond to distributional zero, it is even tempting to postulate if a localized experiment changes  $\hat{\kappa}$  to produce distributional zero and the quantum result as “waveform collapse” [21]. Both resemblances are worth further investigation.

It is also worthwhile investigating if uncertainty bias produces Lamb shift [21].

## 12 Statements and Declarations

### 12.1 Acknowledgments

As an independent researcher without institutional affiliation, the author expresses sincere gratitude to Dr. Zhong Zhong (Brookhaven National Laboratory) and Prof Weigang Qiu (Hunter College) for their encouragement and valuable discussions. Special thanks are extended to the organizers of *AMCS 2005*, particularly Prof. Hamid R. Arabnia (University of Georgia), and to the organizers of the *NKS Mathematica Forum 2007*. The author also gratefully acknowledges Prof Dongfeng Wu (Louisville University) for her insightful guidance on statistical topics. Finally, heartfelt appreciation is extended to the editors and reviewers of *Reliable Computing* for their substantial assistance in shaping and accepting an earlier version of this work, with special recognition to Managing Editor Prof. Rolph Baker Kearfott.

## 12.2 Data Availability Statement

The data set used in this study are all generated in the open-source project at <https://github.com/Chengpu0707/VarianceArithmetic>. The execution assistance and explanation of the above code are available from the author upon request.

## 12.3 Competing Interests

The author has no competing interests to declare that are relevant to the content of this article.

## 12.4 Funding

No funding was received from any organization or agency in support of this research.

## References

- [1] Sylvain Ehrenfeld and Sebastian B. Littauer. *Introduction to Statistical Methods*. McGraw-Hill, 1965.
- [2] John R. Taylor. *Introduction to Error Analysis: The Study of Output Precisions in Physical Measurements*. University Science Books, 1997.
- [3] Fredrik Gustafsson and Gustaf Hendeby. Some relations between extended and unscented kalman filters. *IEEE Transactions on Signal Processing*, 60-2:545–555, 2012.
- [4] Michael J. Evans and Jeffrey S. Rosenthal. *Probability and Statistics: The Science of Uncertainty*. W. H. Freeman, 2003.
- [5] William H. Press, Saul A Teukolsky, William T. Vetterling, and Brian P. Flannery. *Numerical Recipes in C*. Cambridge University Press, 1992.
- [6] John P Hayes. *Computer Architecture*. McGraw-Hill, 1988.
- [7] David Goldberg. What every computer scientist should know about floating-point arithmetic. *ACM Computing Surveys*, March 1991.
- [8] Institute of Electrical and Electronics Engineers. *ANSI/IEEE 754-2008 Standard for Binary Floating-Point Arithmetic*, 2008.
- [9] J. H. Wilkinson. *Rounding Errors in Algebraic Processes*. SIAM, 1961.
- [10] Oliver Aberth. *Precise Numerical Methods Using C++*. Academic Press, 1998.
- [11] Nicholas J. Higham. *Accuracy and Stability of Numerical Algorithms*. SIAM, 2002.
- [12] R.E. Moore. *Interval Analysis*. Prentice Hall, 1966.
- [13] W. Kramer. A prior worst case error bounds for floating-point computations. *IEEE Trans. Computers*, 47:750–756, 1998.
- [14] G. Alefeld and G. Mayer. Interval analysis: Theory and applications. *Journal of Computational and Applied Mathematics*, 121:421–464, 2000.
- [15] W. Kramer. Generalized intervals and the dependency problem. *Proceedings in Applied Mathematics and Mechanics*, 6:685–686, 2006.

- [16] A. Neumaier S.M. Rump S.P. Shary B. Kearfott, M. T. Nakao and P. Van Hentenryck. Standardized notation in interval analysis. *Computational Technologies*, 15:7–13, 2010.
- [17] C. P. Wang. A new uncertainty-bearing floating-point arithmetic. *Reliable Computing*, 16:308–361, 2012.
- [18] J. Vignes. A stochastic arithmetic for reliable scientific computation. *Mathematics and Computers in Simulation*, 35:233–261, 1993.
- [19] C. Denis N. S. Scott, F. Jezequel and J. M. Chesneaux. Numerical 'health' check for scientific codes: the cadna approach. *Computer Physics Communications*, 176(8):501–527, 2007.
- [20] J. Hefferon. Linear algebra. <http://joshua.smcvt.edu/linearalgebra/>, 2011.
- [21] Michel Le Bellac, G Barton. Quantum and statistical Field Theory. Oxford University Press, 1992, ISBN 9781383026535.